Biomedical Signal Processing and Control 39 (2018) 139–161

Contents lists available at ScienceDirect

Biomedical Signal Processing and Control

journal homepage: www.elsevier.com/locate/bspc

Review

MRI based medical image analysis: Survey on brain tumor grade classification

Geethu Mohan [a], M. Monica Subashini [b,*]

[a] School of Electronics Engineering, VIT University, Vellore, 632014, India
[b] School of Electrical Engineering, VIT University, Vellore, 632014, India

ARTICLE INFO

Article history:
Received 11 April 2017
Received in revised form 20 June 2017
Accepted 20 July 2017
Available online 8 August 2017

Keywords:
MRI
Astrocytoma
Brain tumor grade
Segmentation
Neural networks
Classification

ABSTRACT

A review on the recent segmentation and tumor grade classification techniques of brain Magnetic Resonance (MR) Images is the objective of this paper. The requisite for early detection of a brain tumor and its grade is the motivation for this study. In Magnetic Resonance Imaging (MRI), the tumor might appear clear but physicians need quantification of the tumor area for further treatment. This is where the digital image processing methodologies along with machine learning aid further diagnosis, treatment, prior and post-surgical procedures, synergizing between the radiologist and computer. These hybrid techniques provide a second opinion and assistance to radiologists in understanding medical images hence improving diagnostic accuracy. This article aims to retrospect the current trends in segmentation and classification relevant to tumor infected human brain MR images with a target on gliomas which include astrocytoma. The methodologies used for extraction and grading of tumors which can be integrated into the standard clinical imaging protocols are elucidated. Lastly, a crucial assessment of the state of the art, future developments and trends are dissertated.

Contents

* Corresponding author.
E-mail addresses: geethu.mohan2016@vitstudent.ac.in (G. Mohan), monicasubashini.m@vit.ac.in, monicasubashini.m@gmail.com (M.M. Subashini).

http://dx.doi.org/10.1016/j.bspc.2017.07.007
1746-8094/

1. Introduction

Over the past several decades' diseases have fallen before the scythe of human intelligence in the form of biomedical advances in our understanding of various diseases but still cancer, by virtue of its unstable nature, remains a curse to the mankind [1]. A qualified clinician visually examines many types of medical images, further identifies the probable locations and signs of malignant tumors. This is the method followed for non-invasive diagnosis of tumors. Initially, for the detection of a tumor, imaging systems are used to record medical images. The captured images are passed through various software-based algorithms so as to segregate the suspicious region of the tumor from the healthy region in the image.

Image segmentation secludes the infectious region from rest of the image. Treatment planning is assisted when an accurate segmentation method helps to determine tumor size and location. For this purpose, a skilled clinician has to either set the initial conditions or provide training data for classification. Various researches have been carried out to detect many types of the tumor based on the extraction of visual information from medical images.

The current World Health Organization (WHO) guidelines for brain tumor classification [2] are strictly histopathological, which limits clinical application. This constraint triggers the application of medical imaging for diagnosis and treatment planning including more automated methods. The ever-increasing amount of brain MR image data has created new opportunities for neurosurgeons and medical scientists at the same time burden of excessive accurate data analysis and diagnosis has become tiresome [3]. Hence computer-aided diagnosis can be implemented to enhance physicians' diagnostic capabilities and reduce the time required for accurate diagnosis. In current clinical studies and routine, MR images are assessed either by depending on elementary quantitative measures or based on qualitative criteria only. Hence substituting the routine evaluations with greatly reproducible and precise image processing routines and tumor substructure measurements which can automatically inspect brain tumor scans would enhance improved diagnosis and treatment planning. The majority of the current algorithms used for the analysis of brain tumor targets on the glial tumor segmentation [4].

In medical imaging, segmentation is a mandatory task which can be done manually by an expert with good accuracy but time-consuming. At the same time, fully accurate and automatic segmentation approaches are not yet authentic. Currently, for clinical application, partial automatic segmentation methods are adapted. These time consuming and challenging tasks by radiologists' drives towards the demand for a semi-automatic segmentation method. This could alleviate the drawbacks of automatic segmentation method simultaneously the radiologists will also have control over the segmentation process. Several semi-automatic methods need only user initialization. Repeated user interaction is mandatory to assure accuracy.

The review is further structured as follows: Image processing and computer vision (Section 2), where we briefly summarized about Preprocessing, Segmentation (with subsections on Manual segmentation, Semi-automatic and fully automatic methods), Feature extraction, Feature selection, Dimensionality reduction and Classification. Further (Section 3) the current trends in MRI-CAD scheme are explained. Lastly, we discuss the current state of the art in the area of segmentation and classification that would benefit grading of brain tumors and compared it to the clinical requirements.

2. Image processing and computer vision

The field of computer vision has the ultimate goal to use computers to imitate learning and human vision. It also has the ability to form inferences and take action on the basis of visual inputs. The field of image understanding or analysis lies between computer vision and image processing [5]. The general computerized processes are low, mid and high- level processes. Low-level processes involve basic operations like noise reduction by image pre-processing, image sharpening and contrast enhancement. Mid-level processing includes segmentation and classification. High-level processing involves performing cognitive functions normally associated with vision.

Image analysis takes the aid of semi-automatic or automatic methods to illustrate the captured images. The abundance of clinical data generation has made it impossible to manually define and segment the data in appropriate time. The medical image analysis domain is divided into enhancement, registration, segmentation, visualization, quantization and modeling [6]. Among this registration, segmentation and modeling are the most important and challenging when it comes to brain tumor studies.

Despite the expert's experience and skills, the manual qualitative analysis is always bounded by the human vision system. The reason is the inability of the human eye to discriminate between several tens of gray levels [7]. The abundance of information contained in an MR image is much more than what the human vision can visualize because the present MRI systems can produce images equal to 65,535 gray levels [7]. This leads to using the computer as the second eye to play the role of understanding high bit-depth and high-resolution MRI images. For instance, a mathematical framework using both rough sets and fuzzy sets that deals with the uncertainties associated with the human cognition process are studied in [8].

2.1. Pre-processing

A wide variety of pre-processing techniques like linear, non-linear, fixed, adaptive, pixel- based or multi-scale, are applicable for different circumstances [6]. Applications where discrimination between abnormal and normal tissue is delicate, precise interpretations become severe for relatively high noise levels. The small

difference that exists between abnormal and normal tissues might be perplexed by artifacts and noise often resulting in difficulty of direct image analysis. At the same time, some improvement in image visual quality is of great assistance in interpretation by a medical specialist. Hence for subsequent automated analysis, enhancing techniques are one of the pre-processing steps.

Enhancement techniques are used with two aims. Firstly for generating improved images that can be utilized by a human observer. Secondly to derive images to be used in subsequent algorithms for computer processing. Examples of former aim include noise removal, contrast enhancement and sharpening details in an image while that of later includes the former examples extending to edge detection and object segmentation.

A major problem faced during the segmentation process in MR images is the bias field. It is due to the radio frequency coil imperfections or defects in the acquisition sequences and hence called intensity non-uniformity. The aim of correcting bias field is to calculate the bias field and eliminate it from the measured image [8]. The bias correction requirements in an MR image in the pre-processing stage is explained in [8,9].

校正偏置场的目的是计算偏置场并将其从测量图像中消除

Usually, the noise in the MR images is due to the fluctuations of the magnetic field in the coil [10]. The various inhomogeneities associated with MR images are noise, shading artifact, and partial volume effect. The random noises associated with MR images have Rician distribution [11]. Intensity inhomogeneity occurs because of radio frequency non-uniformity during the data acquisition, which will result in shading artifact [11]. When more than one type of tissues or class takes up same voxel or pixel it is called partial volume effect. These pixels or voxels are generally called muxels [12] explains three algorithms for bias field correction.

An inherent trade-off exists between Contrast to Noise Ratio (CNR), Signal to Noise Ratio (SNR) and resolution in MRI applications [13]. High contrast and high spatial resolution are mandatory based on the type of diagnostic tasks. A high SNR is a must in image processing applications as most of the algorithms are noise sensitive. This highlights the need for applying noise filtering on MR images to preserve fine details of image and decrease image noise. Various approaches to improve edge blurring effects, CNR and SNR were proposed in literature such as adaptive filters, anisotropic diffusion filters and wavelet filters. Anisotropic diffusion filtering technique has shown good practical suitability because of its algorithmic simplicity, computational speed and it assumes a Gaussian distribution for noise. But during MR data processing, a Gaussian assumption is not satisfactory for image noise as it shows Rician distribution, notably in low SNR regions. Hence modified anisotropic filters were used to reduce this bias.

图像噪声

Different types of noise corrupt a medical image. But for accurate observations, it is necessary to have precise images for a given application. The procured MR images are generally impaired by speckle noise, Gaussian noise, salt and pepper noise etc. Usually, the main limitation is neglecting local features like presence of possible edges and replacing the noisy pixels by some median value in their proximity. Hence especially at the high noise level, edges and details are not satisfactorily recovered. But image processing analysts affirm that for noise removal in the presence of edges, median filtering is a superior choice than linear filtering [14].

图像标准化

In the pre-processing stage, another step required is intensity normalization. Reference [15] quotes, six such methods for MRI such as intensity scaling, contrast stretch normalization, histogram normalization, histogram stretching, histogram equalization and Gaussian kernel normalization. Comparatively the best performance was given by histogram normalization method but in [16] it says histogram equalization had limited success on medical images as it obliterates the small details. Hence this limitation persuaded the progress of adaptive and spatially variable processing techniques. To be flexible to spatial and local variable details in images, the Wiener filter was optimally designed. It's a combination of low pass and high pass filter with factors controlling its relative weights; hence it is usually applied on Computed tomography (CT) and MR images. In the case of mammographic images, the contrast enhancement techniques that are nonlinear were particularly used but contrast or edge enhancement accompanies with undesirable amplification of noise. Hence a framework based on wavelet was used to implement both de-noising and contrast enhancement [17]. Hybrid filter integrated multi-resolution wavelet transforms with an adaptive multistage nonlinear filter. It addressed noise suppression and image enhancement along with decomposition and selective reconstruction of wavelet based sub-images [18].

In the pre-processing stage, [19] used the N3 algorithm for bias field correction, Statistical Parametric Mapping's (SPM) co-registration module for co-registration between scans for inter-scan visual comparison and a multiplicative model for MR signal intensity normalization. In [20] adaptive histogram equalization was done prior to glioma segmentation in the pre-processing stage where intensity values of the image were made consistent across MR image types, slices and patients. In addition to this, to isolate the pixels of brain tissue from rest of the non-brain pixels SPM5 was used.

T2-w, Proton Density (PD) and FLAIR, are the generally used types of MRI in clinics [21]. These sequences can be fused at two levels namely data and decision level. The former extracts feature from all sources of data and use them for tumor segmentation and in the later firstly segmentation is done in each source of data and then based on some criterion; all the segmentation results are fused. Ambiguity is reduced with more input data hence improving the segmentation but, it leads to redundancy, thereby increasing computation time and affecting the decision.

The separation of tumor sub-regions can merely be possible on a combination of many modalities, which demands a pre-processing step for accurate registration. The majority of algorithms uses some set of pre-processing for image enhancement like de-noising, intensity normalization, and bias field correction so as to balance the effect of magnetic field inhomogeneities, registration and skull-stripping [22].

大多数算法都使用一些预处理来进行图像增强，如去噪、强度归一化和偏置场校正，以平衡磁场不均匀性、配准和颅骨剥离的影响

Another challenge to the algorithms is that the data set may be collected from different MRI scanners and feed as input to the algorithms. This collection consists of MR images of different intensities because the MR image intensities are not consistent across MRI scanners. The other difficulties are MRI scanners producing distinct types of noise, inter-slice intensity variations, problems related to the tumor when aligning and registering images, etc. Many types of pre-processing steps are performed to eliminate these problems. The focus on pre-processing stage of MR images before it is fed to the classifier is important; else a failure in pre-processing stage leads to whole system failure [23].

图像预处理失败，系统就失败

Usually, the background of an image does not contribute any fruitful information at the same time increases the processing time [14]. Hence to improve the processing speed and decrease memory usage, remove background, eyes, scalp, skull, and structures that are not the regions of interest. The Brain Surface Extractor (BSE) algorithm which is used only for MR images can be used for skull removal [14,24]. The images are filtered using BSE removing irregularities, performing morphological erosions, detecting edges and isolating brain. It also does image masking and surface clean up.

The pre-processing step in [25] mainly used skull stripping of T1-w images followed by co-registering of T1-w and T2-w images. The FMRIB Software Library abbreviated FSL has a Linear Image Registration Tool (FLIRT) which was embedded to automatically calculate the transformation between T2- and T1-weighted images for each patient.

Two brain extraction algorithms namely 2D Brain Extraction Algorithm (BEA) and 3D-BEA, for T2-weighted MRIs, are proposed

in [24]. The reason for extraction of the brain from the T2-weighted datasets is to reduce the file size of the MRI and thus decreases the transmission time in a network application. A brain mask is obtained using the Largest Connected Component (LCC) analysis and morphological operations, from which brain is extracted. 2D-BEA employs only 2D information of slices. When the concept of LCC fails for few slices, the available 3D information in neighboring slices is utilized resulting in 3D-BEA. It has been experimentally proved using 20 MRI data sets that 3D-BEA performed exceptionally well when compared to 2D-BEA and other prominent methods like BSE and Brain Extraction Tool (BET).

In [7] many algorithms like BSE, BET, Hybrid Watershed Algorithm (HWA), Minneapolis Consensus Strip (McStrip) etc. were developed for the extraction of brain tissue from undesired structures. Because of the frequency of exclusion and inclusion errors, many of the semi-automatic and automatic brain extraction techniques are not perfect in terms of robustness and accuracy [26]. Out of these McStrip is an automatic hybrid algorithm requiring no user intervention. It is used for nonbrain and brain segmentation having an advantage of integrating thresholding, non-linear wrapping and edge detection.

2.2. Segmentation

目标定位或边界检测、边界估计等都属于分割过程

Object localization or boundary detection, estimation of boundary etc. all belongs to the process of segmentation [27]. Human eyes effortlessly differentiate the structures of interest and extract them from background tissues but in algorithm development, it is a great challenge. Segmentation guides the result of the whole analysis because the proceeding steps depend on the segmented regions. The main principle of segmentation algorithms is intensity or texture variations of images using region growing, deformable templates, thresholding, and pattern recognition techniques like fuzzy clustering and neural networks. Also, techniques like region based and edge segmentation, adaptive and global thresholding, gradient operators, watershed segmentation, hybrid segmentation and volumetric segmentation, supervised and unsupervised segmentation exists. A new approach was based on deformable models which are suitable for images having weak boundaries, artifacts and noise. In this, a model having flexible boundary is kept in the proximity of the region to be segmented and to fit the contour of the region, the model is repetitively adjusted.

Segmentation is accomplished by recognizing all voxels or pixels belonging to the object or by identifying those making boundaries. The former uses pixel intensity and later uses image gradients which have high value at edges. Segmentation is usually considered as a pattern recognition problem as it involves pixel classification.

分割通常被认为是一个模式识别问题，因为它涉及到像素分类

In medical image analysis hybrid approach for segmentation is done initially using the fundamental steps of segmentation followed by time-consuming and robust elaborate techniques. Examples of hybrid algorithms used for fully automatic segmentation of brain MRI include thresholding, histogram analysis, deformable templates and nonlinear anisotropic diffusion.

MRI brain tumor segmentation methods are of two categories based on: generative models (rely heavily on domain-specific prior knowledge about the appearance of both healthy and tumorous tissues) and discriminative models (exploit little prior knowledge of the brain's anatomy and instead rely mostly on the extraction of a large number of low-level image features like raw input pixels values, local histograms, texture features such as Gabor filter banks, alignment-based features such as inter-image gradient, region shape difference, and symmetry analysis). Classically used discriminative learning techniques are Support Vector Machines (SVM) and decision forests [4]. The drawbacks of generative models, as well as the calibration issues related to discriminative approaches, gave rise to the development of joint generative-discriminative methods. Such methods employ a generative technique in the pre-processing step to provide stable input for the successive discriminative model which may be trained to anticipate complicated classes.

One discriminative-generative, one generative and eight discriminative models were used by the participants of BRATS 2013. Out of these, the main learning algorithm used by four participants was Random Forests (RF) [4]. Many of the top-ranked algorithms depended on a discriminative learning approach where, in the initial step local features of the image were produced and then a discriminative classifier was used, which converted these features into class probabilities.

Generally, in segmentation processes, an expert clinician manually outlines the Region of Interest (ROI) with the use of a cursor. The parameter such as threshold has to be automatically set in case of automated computer-assisted segmentation. Even if MR images are from scanners of varying slice thickness, Field of View (FOV) and relaxation times, an automatic technique must be robust so as to generate steady segmentation. Hybrid techniques involving model based methods and image processing are efficient methods for segmentation [6]. Computer-aided techniques having semi-automatic or automatic segmentation methods are used to mark the tumor regions of MR images but the former method employs user defined ROI needing less computational time while the later needs high computational time. So presently in most of the clinical studies, manual segmentation or strict segmentation under the supervision of an expert is carried out. This is because the segmentation performance is affected by the degree of operator administration in terms of time consumed [28]. Hence a necessity of automated method comes up. [29] reviews on methods for Glioblastoma Multiforme (GBM) segmentation from MR images. The highest dice similarity index was for region growing-FCM (Fuzzy C-Means) hybrid and Expectation Maximization (EM).

Segmentation algorithms can be categorized based on the features used. Like the clustering or classification methods that utilize voxel-wise texture and intensity features or the edge- or region-based techniques which use deformable models [22]. Clustering groups data on the basis of similarities and works in an unsupervised manner while classification demands training data to learn a model.

Radiologists with experience and expertise can visually analyze MR images and can make accurate tumor prediction. They differentiate among different tumors based on heterogeneity or homogeneity in texture or by considering hypo-, hyper- or iso-intensity criteria. These features which are extracted visually provide guidelines for finding appropriate descriptors of mathematical feature for Computer Aided Design (CAD). So they take the guidance of a CAD system to eliminate subjective variability, ambiguity and make an objective decision concerning the class of the tumor [30]. [31] Clearly states that the reappearance of tumor growth at the reception boundary is a common aspect, which is another motivation to develop perfect segmentation so that the boundary is defined exactly, resulting in no tissue remains after resection.

2.2.1. Manual segmentation

Traditionally the information obtained by a skilled radiologist, on manual segmentation is highly reliable. Also, the final scrutiny must be done by the medical doctors and they have the ultimate control over the segmentation process. When segmentation was accomplished by various clinicians, the variability analysis among them in segmenting was studied in [32]. From the data of ten patients, GBM was segmented by four clinicians, once manually considering slice by slice, by sketching boundaries and other time employing Slicer's grow-cut segmentation module. The time consumed for manual segmentation was a mean of ten minutes and for

手工分割平均十分钟

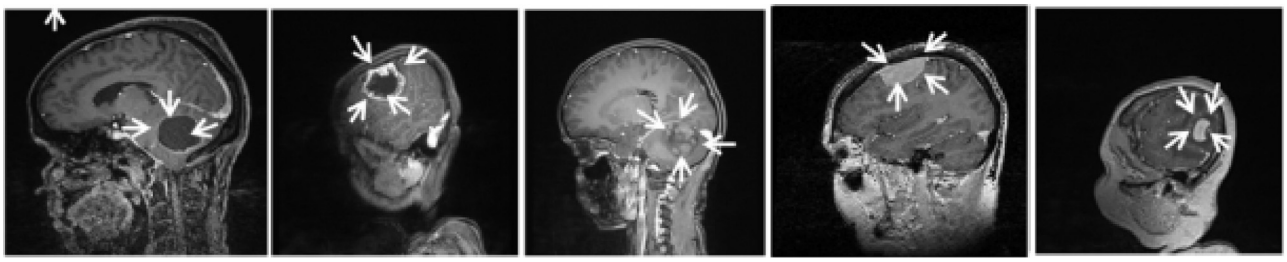

Fig. 1. T1c MR Images exhibiting brain tumors [30] (2-column fitting).

the semi-automatic segmentation using 3D Slicer was five minutes. The time needed for the later was 61% on an average of the time needed for a neat manual segmentation.

手动分割观察者间的差异是缺点

In [20] because of interobserver variations by at most three of four observers, pixels classified as glioma were assessed as real glioma tissue, which highlights a drawback of manual segmentation.

不同时间观察者内的差异

It also quotes 28% inter-observer variability on an average and 20% intra-observer variability when manual tumor segmentation is done over a span of one month.

自动分割的重要性

This shows a clear evidence for the necessity of user independent and time efficient methods for obtaining glioma volume. Manual segmentation was performed by two neuro-radiologists in [25] using ITKSNAP by manually outlining the edges between abnormal areas and normal tissues on the 3D Spoiled Gradient Echo (SPGR) images.

The tumor outer margin is often defined manually by the radiologist on T2 and T1c images by thresholding edges between the hyperintense T2/T1c lesions and the neighboring healthy tissue [22]. Clinical measurements of the tumor size are generally the product of minor and major axis for 2D measurements or that of the three main axes of a tumor in case of 3D measurements. In [17] grading or manual characterization of tumors was done by experts by following various protocols like stereotactic or neuronavigational biopsy, clinical history of the patient, experience, and knowledge in identifying the group of disease from image visual features and at times CT imaging features.

An experienced radiologist uses pathological details to classify brain tumors in MR images. These details are texture patterns which may be heterogeneous or homogeneous and signal intensities which may be iso-, hypo- and hyperintense. Tumors exhibiting iso-, hypo- and hyperintensity have the same intensity as, darker than as and brighter than that of brain tissues respectively. Heterogeneous tumors illustrate varying signal intensity areas like the cystic and the necrotic part inside the tumor while homogenous tumors display comparatively similar signal intensity over their entire area as in Fig. 1 [33].

A final percept is produced by fusing different visual features from 2&3D images by the human cognitive process. So during diagnosis, the perception of the ROI greatly relies on features describing the change in contour, motion, luminance and different 3D cues. These features aid radiologists in analyzing the brain MRI slices [26].

Abundant information is provided by MR images regarding the brain soft tissue anatomy but, this makes manual interpretation difficult. Hence there arises a demand for image analysis tools that are automated [18]. However, manual segmentations are widely used to evaluate the results of semi-automatic and fully automatic methods [34]. But ultimately the completeness of a methodology is assessed by the manual segmentation which is the Gold standard [35].

手工分割金标准

2.2.2. Semi-automatic segmentation

Semi-automatic methods require the interaction of the user for three main purposes; initialization, intervention and evaluation. Initialization could be defining an ROI, containing the approximate tumor region, for the automatic algorithm to process. Intervention is needed to adjust parameters of pre-processing methods. An automated algorithm can be driven towards the desired result by receiving feedbacks and providing adjustments in response. Finally, the user can evaluate the results and modify or repeat the process in accordance with the requirement [34].

For multimodal brain tumors, a semi-automatic segmentation method was presented in [36]. It had advantages of quick segmentation within a minute, easy initialization and efficient modification. A user had to manually sketch ROI approximately covering the tumor. The level set approach, edge and region-based active contours were the image analysis techniques combined in the algorithm.

A semi-automated segmentation method to figure out residual/recurrent tumor volume of GBM, for faster volumetric assessment, was worked out in [37]. Volumetry was performed by manual segmentation and Computer-Assisted Volumetry were compared. The inter-observer correlation was calculated among volumetric, 2D and 1D technique. Dataset of 29 patients who had GBM was analyzed. Disagreement in the status of disease between 1D and 2D, when correlated with computer-assisted volumetry, was 3/29 and 5/29, respectively. Less than 1 min and 9.7 min were the segmentation mean time for computer-assisted volumetry and manual methods respectively. Volumetric measurements gave the highest inter-observer correlation compared to 1D and 2D measurements. Their work concluded that fast and reproducible volumetric assessment was possible using computer-assisted volumetry.

手工与机器分割时间差距

AFINITI (Assisted Follow-up In Neuro-Imaging of Therapeutic Intervention) is a semi-automatic software pipeline for the segmentation of GBM proposed in [25]. Both the benefits of voxel-based and deformable shape-based segmentation algorithms were embedded into the software pipeline. It took approximately 20, 4, less than 1 min for the automatic process, interactive refinement process and for output without correction respectively for each dataset. But for manual segmentation, the time varied from 30 to 90 min based on the tumor characteristics. The AFINITI software pipeline is freely available on the web.

The Random Walker algorithm with priors (RW PR) is an interactive segmentation tool which was tested on 3D CT image of the knee [38]. User interaction is repeatedly needed to assure improved accuracy even though most of the semi-automatic methods have only user initialization. There is a need to quicken these techniques, specifically in 3D, so as to reduce the time consumed for receiving input information and obtaining the output. This refereed work explains a method to speed up semi-automatic method which is slow due to human intervention.

An inability often noticed in automatic tumor segmentation methods is that they cannot segment complex boundaries of heterogeneous tumors and consumes high computational time. But they work well to segment solid homogeneous tumors or those with peripheral enhancement [33]. At the same time since ROI is

user defined for semi-automatic methods, it consumes less time for computation [39]. Results in [20] indicate that tumor volume measurement, for determining tumor growth quantitatively by use of both automatic and manual segmentation routine is not adequate. Other methods like adaptive template-moderated classification or threshold-based, semi-automated methods may be used for quantification of tumor volume, invasion and growth.

2.2.3. Fully automatic segmentation

As MRI is associated with a huge information repository, manual interpretation of each image becomes impossible, paving way for automated tools development [16]. In Fully automatic methods, the tumor contours are obtained without any human intervention and are very attractive in theory. When the type of tumor doesn't fit the segmentation model as learned from the training dataset, the segmentation result may be erroneous. Researchers [36] proposes an algorithm that automatically segments brain tumors using Markov random field model, based on super-voxels and terms that capture the intensity probabilities and edge cues. Another research [40] shows an automatic segmentation for high-grade gliomas including their sub-regions at the same time differentiating between edema, necrotic core and active cells. This discriminative approach relied on decision forests. The validation was done on two cases of grade III tumors and 38 cases of grade IV tumors obtained from multi-channel MR images. These automatic outputs were suitable for measurement of tumor volume and aided interactive treatment planning.

A study aiming at recurrent glioblastoma was proposed in [19] to improve efficiency and accuracy of treatment response assessment automatically. A modified k-Nearest Neighbor (kNN) classification method was used on 59 longitudinal MR Images from 13 patients to assess the changes in tumor volume. This method was then compared with manual volumetric measurements and Macdonald's criteria. Even for all scans with infiltrative tumors having unclear borders, this method was suitable. A high correlation existed between the manual tumor volume measurements and the automatic method ($r = 0.96$) but their match with Macdonald's criteria was only 68% even though these outputs were validated using Magnetic Resonance Spectroscopy (MRS) as well as by a neuro-radiologist.

Research [20] characterized gliomas from Dynamic Susceptibility Contrast (DSC) imaging, to find out whether tumor volume is calculated using FCM clustering gave identical diagnostic efficiency as the manual definition of tumor volumes. It took nearly 4 min to produce a binary glioma volume per patient by this method and 10 min manually. When the low-grade and high-grade glioma volumes were compared, the automatic method showed greater sensitivity than manual method: 83% for low-grade gliomas and 69% for high-grade gliomas. Although DSC imaging shows possibility in the characterization of gliomas prior to surgery, these methods are confined to leading research-oriented institutions only.

Automatic tumor segmentation using multi-spectral data analysis [19], Artificial Neural Networks (ANN) [16,41], SVM [27,33,42–44] and knowledge-based FCM clustering [20] techniques are promising methods. The benefits of performing tumor segmentation automatically are efficiency in time, the absence of inter- and intra-observer variability and tumor characterization using consistent benchmarks.

2.3. Feature extraction

Feature extraction can be defined as the process of transforming or converting an image into its group of features. The different methods employed for feature extraction includes texture features, co-occurrence matrix, Gabor features, wavelet transform based features, decision boundary feature extraction, minimum noise fraction transform, nonparametric weighted feature extraction and spectral mixture analysis. For feature reduction principal component analysis, linear discriminant analysis and independent component analysis are used. Integration of the feature extraction with the feature reduction algorithms leads to accurate systems that use less number of features that can be extracted with less computational cost [16,45].

The tumor type and grade are the two main factors that decide the features used for brain tumor segmentation. This is because diverse types and grades of tumor exhibit variations in appearance that may be shape, location, regularity, contrast uptake etc. The commonly used features are the image intensities assuming that different tissues have varying gray levels. Local image textures are one more type of features generally used since different areas of the tumor shows varying textural patterns. The features based on alignment use spatial prior knowledge. The combination of alignment-based and textural features showed considerable improvement in performance. For growing a contour towards the tumor frontiers, edge-based features or intensity gradients can be used [22].

For feature extraction, texture can be modeled as a 2D array of gray level variation. Such a pattern matrix employed to find the image texture pattern is called a Gray Level Co-occurrence Matrix (GLCM) [46]. This statistical method is otherwise called gray-level spatial dependence matrix as it provides the spatial relation between pixels. The image is analyzed on different resolution scales in wavelet feature extraction which uses wavelet transform. Then the image is converted into a multi-resolution image with many frequency components. After this conversion, the image spatial and frequency characteristics can be analyzed together.

The key feature recognition is a crucial aspect of designing an efficient expert system. Astrocytoma grade determination is possible when the algorithm can find characteristics of tumor considering patient age also as a feature. Indeed features are extracted so as to decrease memory, time and data [47]. Feature extraction is essential because results are directly computed based on the extracted feature data [3]. Effective discrimination of features make up an optimum feature set simultaneously reducing redundancy of feature space to avert dimensionality problem [16].

Traditionally used features like image intensities, textures, edges, and alignment doesn't necessarily associate with actual anatomical meanings of a brain tumor because for the same patient, same body region using the same scanner, MRI intensities within the same MRI modality may differ. Hence obtaining additional features that denote relevant anatomical meanings for tumor is of significant importance in tumor segmentation. Wavelet transform, Independent Component Analysis (ICA) and Fourier transform can be used for obtaining essential features from MR images [18].

In assessing gliomas various diagnostic factors that are non-pictorial like calcification, blood supply, hemorrhage, edema and age have taken importance. The most modern studies utilize MRS features or combination of spectroscopic and textural features to differentiate among brain tumor types. Whether the studies employed the latest classifiers or statistical analysis methods, MRS features have proved in providing an added value in precise brain tumor characterization [48]. Some techniques are based on extremely high dimensional features which pose difficulty in terms of memory storage [23]. Feature extraction plays a crucial step in segmentation process because extracting feature set is complicated as features vary from one image to another image [49].

2.4. Feature selection and dimensionality reduction

The existing methods utilize not many features for portraying the tumor pathology and none of the works used the entire features

in an exhaustive manner. But, the use of complete heterogeneous information resulted in high-dimensional feature vectors that considerably decreased the system accuracy. Hence, to design robust brain tumor descriptors of appropriate size that decreases unimportant information, a reliable feature selection method is to be adopted.

More efficient techniques use lesser number of features, using dimensionality reduction, but the reduction in the number of features is often at the cost of reduced accuracy [41]. Feature selection algorithms popularly used are Genetic Algorithm, Sequential Backward Selection (SBS), Sequential Forward Selection (SFS), and Particle Swarm Optimization (PSO) [45], while Principal Component Analysis (PCA), kernel PCA and ICA help in dimensionality reduction [21]. Feature selection improves the efficiency of learning models by reducing the effects due to the curse of dimensionality, hastening learning process, improving generalization capability and enhancing model interpretability. Neglecting this stage leads to huge dimensionality in feature space and poor classifier performance [50].

特征选择通过减少维数灾难的影响，加快学习过程，提高泛化能力，增强模型的可解释性，提高了学习模型的效率。忽略这一阶段会导致特征空间的维数过大，分类器性能较差。

According to [51], the most popular methods of feature selection are PCA, ICA, and Genetic Algorithm (GA). PCA converts feature space of input into a feature space of lower dimension using largest eigenvector of the correlation matrix. While ICA converts it into a feature space of dimensions that are independent of each other. GA searches for the optimal feature set by evaluating the search results on the basis of an evaluation function. This evaluation function computes how appropriate the chosen features are for the classification problem.

When the aim is to convert the input feature set having many interrelated variables into a lesser dimension, at the same time retaining most of the variations to process the data faster and effectively, PCA is the suitable approach [52]. While performing PCA, it is usual to maintain a minimum set of principal components having at least 97% of the variance.

Many methods used for feature selection was explained in [53] which are appropriate for biomedical image classification. Three different techniques are analyzed namely Multiple Kernel Learning (MKL) which excludes feature subsets having similar attributes, a GA based approach having an SVM as decision function and Recursive Feature Elimination (RFE) using many classifiers. The best technique suggested was SVM-RFE although MKL uses lesser number of features. The RFE technique focused on co-occurrence matrix features at the cost of extreme instability in the selected number of features while MKL selected wavelet based texture features.

In statistics and machine learning, the most important and appropriate information can be acquired by feature selection. The work [42] explains three main methods for feature selection namely wrapper model, embedded model and filter model. First is the filter model having the advantage of low cost but it fully avoids the impact of the learning algorithm. Due to the filter models' disadvantage, came up the second category, the wrapper model which considered the interaction between the training set and algorithm. Even though wrapper models gave increased accuracy, it is computationally expensive. Then learning algorithm was integrated with weighting procedure or variable selection in case of embedded methods.

A feature selection technique having two steps of feature ranking and selection is proposed in [54]. On the basis of each features discriminating power, the feature ranking method calculates a rank per feature. Further, the features possessing top rank are sustained so as to create a feature vector having only the relevant features. Dissimilarly, the feature selection method removes redundant features and concentrates on selecting discriminative features. Hence merging feature selection and ranking results in fewer features by excluding redundant and irrelevant features. This combination gave better classification accuracy than compared to the application of feature selection method alone.

Further dimensionality reduction increases the classification accuracy; even though kernel-based methods are less sensitive to input space with high dimension. To handle smaller data sets and input space with higher dimension SVM is the common technique [42]. As stated in [49] some of the extracted features may degrade the classifier performance and all the features may not be discriminant enough on all the images. In reality, the process of extraction and selection of features plays a vital role in determining the segmentation performance.

2.5. Classification

In some approaches, segmentation problem is transformed into a classification problem and a brain tumor is segmented by training and classifying. Generally, a machine learning classification method for brain tumor segmentation requires large amounts of brain MRI scans with known ground truth from different cases to train on. Mainly, artificial intelligence and prior knowledge are combined to solve the segmentation problem. Currently, high segmentation performances are obtained by deep learning methods [34].

目前，通过深度学习方法可以获得较高的分割性能

Factors of consideration in the design of an optimum classifier include (a) classification accuracy, (b) algorithm performance, (c) computational resources [16]. The brain MRI classification is achieved using supervised techniques like ANN, SVM, k-NN and unsupervised classification techniques such as Self Organizing Map (SOM) and FCM.

最佳分类器时要考虑的因素包括：(a) 分类精度，(b) 算法性能，(c) 计算资源

Automatic brain tumor segmentation can be of two types namely discriminative and generative methods. Previous studies indicate that methods based on discriminative classification were the best performing in general among other automatic methods [34,36]. Discriminative methods learn the relationship between the input image and the ground truth by relying on features and feature extraction [40]. In most cases, they use supervised learning techniques requiring large data set with the valid ground truth. On the other hand, generative methods generate probabilistic models by using prior knowledge like location and spatial extent of healthy tissues. Previously obtained atlases of healthy tissues are used to extract the unknown tumor compartments [34]. However, converting prior knowledge into suitable probabilistic models is a complicated task.

Steps followed by the discriminative method of segmentation are pre-processing, feature extraction, classification and post-processing steps.

1. Pre-processing step usually include noise removal, skull-stripping and intensity bias correction.
2. After pre-processing, image processing techniques are employed to extract features that represent each distinct tissue type effectively. Features like intensity, texture, asymmetry-related features; Discrete Wavelet Transforms (DWT), textons, multifractal Brownian motion features, first order statistical features, intensity gradients and edge-based features are some examples.
3. By using these features different types of classifiers; SVM, Neural Networks (NN), kNN, SOM, RF are implemented.
4. In some cases, results of the segmentation are refined to increase performance. Conditional Random Fields (CRF) and Connected Components (CC) are among the popular choices.

In contrast to traditional classification methods, in which extracted features are fed into networks, Convolutional Neural Networks (CNN) automatically learn representative complex features directly from the data itself. Hence, research on CNN based brain tumor segmentation mainly focuses on network architecture design rather than image processing to extract features. CNN take

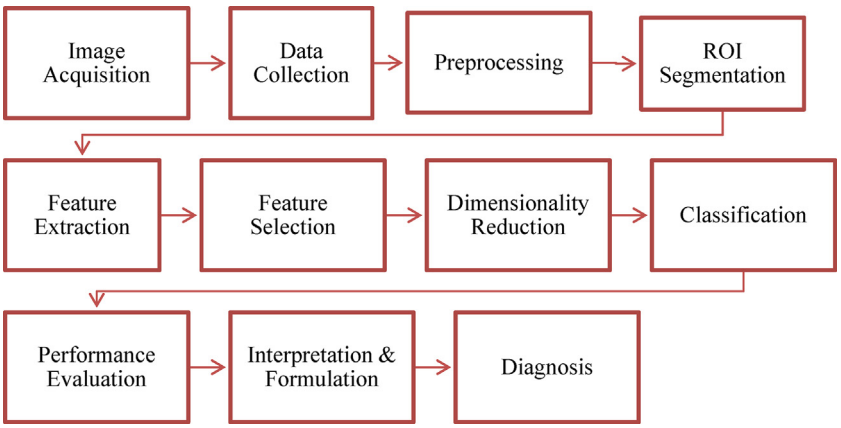

Fig. 2. Typical methodology of MRI-CAD schemes (2-column fitting).

patches extracted from the images as inputs and use trainable convolutional filters and local sub-sampling to extract a hierarchy of increasingly complex features [34].

3. Current trends in MRI-CAD scheme

The following section gives detailed methodology of various CAD schemes used for brain tumor classification. The methodologies are subdivided into categories as fully automatic and semi-automatic 2D & 3D user interaction methods. In all the methodologies the framework is as shown in Fig. 2.

3.1. Fully automatic 2D & 3D user interaction methodologies

3.1.1. Fuzzy logic

A type-II Approximate reasoning method was used with a combination of the median, unsharp masking and Wiener filter for preprocessing in [28]. The results after preprocessing were sharpened edges, reduced noise, and the overall output was superior to that of using a single filter. The system determined tumor using abnormality cluster and the mass effect using the Cerebrospinal Fluid (CSF) cluster. For approximate reasoning, the rule base considered three parameters namely patient age, tumor shape (mass or cystic) and mass effect existence. When considering the tumor shape if it is mass, the tumor could be grade III or II and if they are cystic then it could be grade IV or I.

In [10] segmentation is done using FCM and K-Means clustering method. Out of both FCM clustering produces better segmentation. Classification is done by using the Generalized Regression Neural Network (GRNN), Radial Basis Function (RBF), Probabilistic Neural Network (PNN) and Fuzzy Probabilistic Neural Network Classifier (FPNNC). It was concluded that even though the computation time was high for FCM, mean square error was less for FCM than K-Means method. Hence, the accuracy was higher for FCM comparatively.

It is lucidly depicted in [55] that the use of a single plane of a single patient gives insufficient information about the tumor. The focus was on developing automated tumor detection for differentiating Astrocytoma from MR image by using an interval Type-2 fuzzy system. The preprocessing is carried out using Type-2 Fuzzy Image Enhancement (T2FIE) technique and segmentation using Interval Type-2 Fuzzy set theory and relative entropy. Collaborative Fuzzy Clustering (CFC) is used for feature extraction. In approximate reasoning step, an astrocytoma is detected and differentiated based on the features extracted by firing eight defined rules.

In contrast, a fully automatic classification method for MR images employing Multi-scale Fuzzy C-Means (MsFCM) i.e. robust to low-contrast and noise is proposed in [9]. After anisotropic diffusion filtering, the MsFCM algorithm does classification from coarsest to finest scale. The class types have to be initially estimated as it is an iterative algorithm. Images having distinct quality were synthesized so as to verify the algorithm on poor contrast images. It is seen that FCM and Modified Fuzzy C-Means (MFCM) gave a poor performance as contrast decreased, while MsFCM still achieved more than 80% overlap ratio.

For neovasculature assessment and brain tumor detection, a multi-stage automatic method is proposed in [56] using six main stages. The series of MR images are registered by means of brain symmetry. The low and high-grade gliomas are differentiated using relative Cerebral Blood Volume (rCBV) perfusion maps. The first limitation of this method is that manual correction is needed for the detection of brain symmetry line and registration, particularly in circumstances when the tumor affects the brain fissures. Secondly, automatic determination of rCBV threshold may be impossible. During diagnosis, a skilled radiologist must examine its value. An advantage is that for each examination the threshold can be updated in the CAD workstation. In this work, a differential image approach is used for tumor segmentation and Kernelized Fuzzy C-Means (KFCM) approach is applied for extraction. The rCBV is an indicative of tumor angiogenesis. MR series are still successfully being practiced as a differential diagnostic tool and hence as of now Perfusion Weighted Images (PWI)/rCBV is hardly used for brain tumor segmentation.

A similar motivation was used for low/high astrocytoma tumor grade identification non-invasively using MRI in [47]. This work focused on grade determination solely from MR images rather than using biopsy or MRS. The automatic selection of dominant parameters is done using Shuffling Frog Leaping Algorithm (SFLA). It is a technique that combines advantages of PSO algorithm and Memetic Algorithm (MA). Results revealed that shape based features have maximum applicability. In this work compared to other features, area showed much differentiation among the two grades. So area calculation was a major factor, as tumor size greatly determined its grade. The FCM segmentation was concluded to be the best solution for tumor grade identification among other methods. It was also deduced that the Naive Bayes classifier could classify at a time only one image while Learning Vector Quantization (LVQ) and SVM classifiers could be applied for bulk image classification.

A hybrid clustering method using K-means combined with FCM algorithm is used for image segmentation in [14]. The proposed technique has benefits that K-means was able to find a tumor quicker than FCM but FCM found tumor cells that went undetected by K-means. Especially for malignant tumors, K-means suffered from incomplete tumor detection but the algorithm works well on large data sets and is simple and fast for the same. FCM, when

compared to K-means, retains more information about the original image for accurate malignant tumor detection. Research [8] proposes a generalized rough FCM for MR images with intensity inhomogeneity to segment it into the background, CSF, White Matter (WM) and Grey Matter (GM). FCM and rough c-means were combined in this hybrid clustering approach.

3.1.2. Adaptive neuro-fuzzy inference system

The distinction of brain anomaly from normal brain tissue is done using Adaptive Neuro-Fuzzy Inference System (ANFIS) on the basis of automatic seed point selection range in [46] but in the referred work [57] it classified the brain tumor regions into benign and malignant, also in [50] into 5 types of brain tumors. For preprocessing, [46] used an anisotropic diffusion filter that preserved the edges and removed noise. Features used were GLCM, Local Binary Patterns (LBP) and wavelet characteristics which are used to train the ANFIS. The other inputs to ANFIS included extracted features from pathological images, tumor area, homogeneity and entropy. In [57] image components were extracted from the binary image using morphological filtering. For accuracy improvement, the post-segmentation process was done using the morphological operations like morphological opening, closing, dilation and erosion. An advantage of ANFIS is its fast convergent time. The ANFIS uses fuzzy rules and fuzzy reasoning that is based on fuzzy set theory. ANFIS is compared with ANN and kNN in [50].

Similarly an image segmentation technique [45] for locating Astrocytoma brain tumor grade I to IV proceeds firstly with preprocessing, feature extraction using GLCM, feature selection (GA + fuzzy rough set) and finally image segmentation using ANFIS. Two membership functions (high and low) were used in this work along with 100 if-then rules forming the ANFIS input.

3.1.3. Support vector machines

Detection and delineation of tumor slices and tumor area respectively were done by a fully automatic system in [15]. The histogram inequality among the brain hemispheres is used for tumor slice detection hence the limitation comes when the tumor is in the midline. Regarding feature extraction, initially spatial, frequency and multi-resolution texture information was provided by the Gabor wavelet method which captures locality, frequency and orientation. Then the statistical method applied Gray Level Run Length Matrix (GLRM), GLCM, LBP and Histogram of Oriented Gradient (HOG). The intensity relation among pixel groups or two image pixels was demonstrated by these feature extraction methods. It was also concluded that with the application of texture based features, noise reduction decreased the classification accuracy.

Similarly characterizing MR images into malignant or benign tumors was done by an automatic CAD system based on a group of classifiers in [54]. Using histogram analysis, the number of clusters in the brain was determined. 3D and 2D tumor features were extracted to evaluate effective differentiation among malignant and benign tumor using Haar wavelets. The feature selection was done using ICA and feature ranking using information gain. The prediction of class was done by combining the decision of multiple classifiers like ANN, kNN and SVM. For this purpose the three classifiers decision was integrated using combination rules of the product, sum, median and mean. Lastly, the image is labeled to the class with the greatest value. This method took 12 s with complete feature vector and 4–5 s with reduced feature set respectively for brain tumor characterization.

In [3] by using the correlation between deformation of brain Lateral Ventricles (LaV) and compression from brain tumors, the LaV deformation is measured and transformed from the 2D images in axial view into feature data. The proposed method applies dynamically created template LaVs by taking advantage of brain hemisphere symmetry. The proposed method aligns and models LaV deformation through 3D viewing. For separating CSF tissues, a dynamically wavelet-incorporated FCM (dwFCM) is used. An assumption is made in this work that in most brain tumor-affected cases, the tumor and edema exist in one hemisphere and with this assumption; the template image is obtained by mirroring the less tumor-affected hemisphere.

Brain segmentation using Vector Field Convolution (VFC) active contour model followed by classification of brain tissues into GM, WM and CSF is done by three SVM classifiers in [27]. The anisotropic diffusion filter was used to correct radio frequency inhomogeneity which is an iterative filter. The Euclidean distance between pixels and intensity squares were useful and simple features were used for brain segmentation. Research [8] concluded that these features showed better outputs only in the absence of intensity nonuniformity and high noise, so substituting them with statistical features can provide a better result.

Three analytic approaches to eliminate features that had no or less impact on classification were proposed in [43]. They were namely, PCA, ICA and Pearson's Correlation Coefficients (PCC). The patient age and whole-tumor Cerebral Blood Volume (CBV) histograms were used for tumor grading using SVM with RBF kernel approach. PCA gave the best classification accuracy of 85% when decreasing the feature vector to 3 from 101 principal components. In this work, age is the best predictor as it has no relation with other features and not a hemodynamic parameter.

3.1.4. Artificial neural networks

The moment invariant feature extraction was used to classify MR images as malignant, benign and normal using NN classifier by [58]. Based on 7 rotation invariants using cubic order differentiations, the different image features were extracted. Feature selection is done by rule pruning techniques based on binary Association Rule (AR). It combines high-level knowledge provided by specialist and extracted low-level image features. It excludes rules that are conflicting and the features selected by the rule pruning technique are the input to the classifier. An advantage of this work was that moment invariant feature extraction method does shape distinction on the basis of few exceptional features. In this AR based NN classification, the features extracted were reduced from 7 to 3. A disadvantage of AR method is in identifying rules that give minimum support values and minimum confidence provided by the user.

DWT is used for obtaining the MR image features, followed by feature reduction using PCA and finally classification by two classifiers namely kNN and Feed Forward Back Propagation Network (FFBPNN) in [59]. Image analysis at different resolution levels is done using an efficient tool for feature extraction i.e. the wavelet transform but at the cost of computational expense and huge storage. Simultaneously for dimensionality reduction of the feature vector and increase of the discriminative power, PCA was used. The input matrix size was reduced to 7 from 1024.

An automated brain tumor grade classification employing Feed Forward Neural Network (FFNN), Multilayer Perceptron (MLP) and Back Propagation Neural Network (BPNN) is proposed in [60]. The features of the brain tumor grades are extracted using GLCM and GLRM. GLRM is the successive pixels having similar gray level intensity along certain orientation and GLCM extracts statistical features of second-order. In GLRM fine textures have a short run with similar gray level intensities while coarse textures consist of long run of varying intensities. Fuzzy entropy measure is used to select the optimal features. Compared to other classifiers BPNN outperforms them with 96.7% classification accuracy.

To prepare the training data, thirteen Harlick texture features were extracted from each MR image. This data was introduced to three ANNs (FFBPNN, Recurrent and Elman network) as input and target vectors [61]. Results explain Elman Network, with log sig-

moid activation function, to be the best among other ANNs with a performance ratio of 88.24%.

In another work, an automatic brain tumor detection and segmentation method using ANN to classify the grade of the tumor proposed in [62] giving an accuracy of 95.30%. To remove the salt & pepper noise, commonly seen in MR images, the median filter is used. Fast Bounding Box (FBB) method was used for Brain tumor detection. Here tumor is classified by feeding 10 features for training ANN. The target matrix is Grade (II–IV), only 3 grades.

The intensity histogram is calculated for each 2D MR image and on this histogram signal Slantlet transform is applied for feature extraction [63]. The magnitudes of Slantlet transform outputs correspond to six spatial positions which create the feature vector per image. The binary classifier based on neural network is trained by these features that automatically make inferences if the image is an Alzheimer diseased pathological brain or normal brain. In the training phase, fast convergence is provided by Levenberg–Marquardt algorithm, a fast variant of BPNN. This work envisages that even if the classifier input is as low as 6 features, it showed considerable improvement in accuracy and its accuracy was compared with the methods in [18].

Classification of brain MR images into abnormal or normal was done using a Scaled Conjugate Gradient (SCG) that calculates the best weights of the BPNN in [64]. Since the weights are adjusted in the direction of steepest descent for basic backpropagation algorithm which does not give fast convergence, SCG algorithm is used. Wavelet Transforms (WT) representing a windowing method with variable size is employed for feature extraction hence, preserving signal frequency and time information. The three levels of wavelet decomposition greatly reduce the input image size. Even though the features extracted were decreased to 1024 from 65536, it was too large for calculation. Hence to do further dimensionality reduction of features to 19 principle components, PCA was used followed by the BPNN.

PCA for feature extraction and PNN for classifying brain tumor into three classes of benign, malignant and normal were utilized in [65]. Further, the malignant tumor is labeled as Meningioma and Glioma.

A hybrid, inexpensive and non-invasive machine learning method to detect brain tumor automatically from MRI was proposed in [16]. Whenever the image database size has increased this work required fresh training. In this technique pre-processing was done by the median filter and high pass filter, image segmentation by Feedback Pulse Coupled Neural Network (FPCNN), feature extraction by DWT, dimensionality reduction by PCA and classification of inputs into abnormal and normal images by the feed forward BPNN.

A method employing CNN for automatic segmentation using 3*3 kernels is proposed in [66]. CNN operates over patches using kernels providing benefits of being less prone to over-fitting because small kernels have lesser weights compared to big kernels. A deeper architecture is used for High-Grade Glioma (HGG) than that for Low-Grade Glioma (LGG) because a deeper architecture does not give better results for LGG. Going deeper for a smaller training set of LGG means including more layers with weight but may result in increased over-fitting. Around 335,000 and 450,000 patches were extracted for training CNN for LGG and HGG respectively. Approximately four times these numbers were obtained as effective training samples with data augmentation.

A similar approach in [67] investigates brain tumor grading employing multiphase MR images and the results were compared with BPNN and CNN. The kernels were trained in distinct layers and they provide some self-learned features attained from CNN. A main advantage of CNN is that the kernel learned from the unsupervised learning process and it functions as the noise suppressor as well as the feature enhancer of the model. An uneven distribution of training class may cause failure of CNN. For deep learning machine, a key factor is training sample size.

Another method using deep learning was proposed in [41]. The reason for using CNN was the advantage of more global contextual features as well as local features simultaneously. The model iterated over about 2.2 million examples of tumorous patches and goes through 3.2 million examples of the healthy patches. The time needed to segment an entire brain varied between 25 s and 3 min. As BRATS dataset lacked resolution in 3D, this model processes sequentially each 2D axial slice, where each pixel is associated with different image modalities. One disadvantage of the CNN is that they predict each segmentation label separately from each other. The advantage is that the two-phase training procedure allows the model to learn from a more realistic distribution of labels [41].

3.1.5. Self-organizing maps

An automated hybrid Self Organizing Maps with Fuzzy K-Means (FKM) algorithm, to identify malignant and benign tumor was proposed in [35]. In this method, clustering performs the segmentation process disintegrating edema portion and tumor region also. Two staged clustering is done, once by SOM and then by FKM. Advantages of this work were that for performance enrichment of FKM algorithm the SOM undertakes the initial level clustering. Faster convergence is provided by the Greedy K-means algorithm in FKM. Also in the case of HGG, the variable dimensions of tumor region were exactly identified with this combined algorithm.

Wavelets are input to neural network SOM and SVM for classification of MR brain images as either normal or abnormal in [18] giving an accuracy of 94% for the former and 98% for SVM. Being an unsupervised algorithm, SOM can automatically form similarity diagrams and produce abstractions, which is an advantage over other networks. The level-2, Daubechies-4 (DAUB4) wavelet decomposition of an MR image was the most convenient for the classifiers. Compared to linear and polynomial kernels, the classification accuracy is higher in RBF kernel. Though DAUB4 wavelet is computationally expensive, it provides improved resolution compared to the Haar wavelet.

The commonly used segmentation methods apply a priori knowledge regarding voxel classification. This inhibits identification of new tissue classes that are distinct from the classes with which the system is trained. Another work [7] proposed two unsupervised methodologies to overcome this inhibition. From the whole volume histogram, appropriate information is extracted and SOM processes this in the first approach while the second approach includes four stages. In the second approach, using overlapping windows, the second and first order features are extracted, feature selection by evolutionary computing and lastly grouping is done by SOM clustering algorithm. The former approach is quick while the later method is robust under bad intensity or noisy conditions. The feature space dimension reduction is done using GA.

A completely different combinational method is proposed in [68] which segments and labels T1-w images using supervised LVQ and unsupervised SOM. To improve quality before segmentation, an anisotropic filter preprocessing is done. The combinations of Stationary Wavelet Transform (SWT) and its statistical features give a multidimensional feature vector which is the input for SOM. The competitive SOM approach is used to segment images and the LVQ system fine tunes this work.

A segmentation method for neuroanatomical analysis based on the Growing Hierarchical Self Organizing Map (GHSOM) with probability-based clustering scheme and multi-objective-based feature selection called GHSOM-Multi-Objective Optimization (GHSOM-MOO) is proposed in [49]. GHSOM is a variant of SOM allowing inherent hierarchies to be discovered and classifying data in an unsupervised manner. The drawbacks of basic SOM were overcome by GHSOM which is a non-fixed and hierarchical structure. An

overlapping and sliding window is used for feature extraction per slice; PCA and multi-objective optimization with Non-dominated Sorting Genetic Algorithm (NSGA-2) algorithm for feature selection. The average overlap values of features calculated by NSGA-2 are greater than the ones from PCA, proving NSGA-2 optimization process to be performing superior to PCA, in dimensionality reduction.

3.1.6. Particle swarm optimization

Reference [69] compared three automated diagnosis systems to detect glioma and classify them into healthy and unhealthy brain images. Four steps are involved per glioma diagnosis system. Firstly, the segmentation of image with PSO, Darwinian Particle Swarm Optimization (DPSO), or Fractional Order DPSO (FODPSO) to obtain image geometric silhouette. Secondly, the Directional Spectral Distribution (DSD) signature of the segmented image is computed. Thirdly, feature extraction of the DSD by means of Multi-Scale Analysis (MSA) using Generalized Hurst Exponents (GHE). Lastly, classification of the obtained multifractal features using SVM. This method has the advantage that it is simple to implement, requires only six multi-fractal estimates used to form the vector of features and takes only four seconds for processing a given brain MRI. The FODPSO-DSD-MSA glioma diagnosis system performed the best. The overall processing time is less than 5 s.

The science of MRI and MRS-based on multi-dimensional co-occurrence matrices is combined in [70]. It illustrates edema and tumor segmentation as well as grading of HGG and LGG. The feature from MRI and MRS are used to train Extreme Learning Machine-Improved Particle Swarm Optimization (ELM-IPSO) neural network classifier. The tissue classes and tumor grades are distinguished using volumetric features and spectroscopic metabolite ratios. Spectroscopic and/or textural features were used to design the ELM-IPSO classification system. Another work [70] clearly highlights that the classification by combining multimodal proton MRS and morphological MR images of the brain is still a challenging task. This is because both anatomy and pathological diagnosis require intensive manual interaction for segmentation and classification.

An MR brain image is classified into normal and abnormal using an FFNN in [71] using a level-3 decomposition via Haar wavelet transform to extract features from images, followed by application of PCA. The dimensionally reduced features are given to FFNN, and optimization is done by Adaptive Chaotic Particle Swarm Optimization (ACPSO). FFNN is a supervised classifier which is trained in this work using PSO. Computationally less expensive PSO needs very few lines of implementation codes and less computational bookkeeping. To obtain FFNN's optimal parameters and for performance improvement of PSO, an ACPSO method was used in [71]. Out of the three types of cross-validation methods (*K*-fold cross-validation, leave-one-out validation and random subsampling), the *K*-fold cross validation with K = 5 was used.

3.1.7. Random forest

Characterization and delineation of four distinct brain tumor types from slices of a T1c sequence of MRI were proposed in [17] using an ensemble learning scheme, RF. A Correlation-based Feature set Selection strategy (CFS) generates reduced set of features on which the same experiment was repeated. Fast computation, large dataset dealing capability and evaluation of potential features were the advantages of RF. The CFS reduced the feature dimension from 86 to 15. The out-of-bag classification error was 0.044 while 0.0278 after dimensionality reduction. Using the entire feature space, RF gave improved results compared to the application of feature selection strategy. The advantages of this methodology were that it required no preprocessing, neither registration nor denoising and also from a single sequence MRI diagnosis was possible.

A supervised segmentation framework based on RF derived probabilities using multiple modality intensity, geometry, and asymmetric feature sets are portrayed in [2]. The ANTsR package is used to interface RF model's supervised learning capabilities with regularized probabilistic segmentation. This package is a comprehensive visualization and statistical interface among the R statistical project and Advanced Normalization Tools (ANTs). Voxel-wise classification with Gaussian Mixture Modelling (GMM) was done. It was applied to model 7 brain/tumor tissue types.

For multispectral and single MR image segmentation in real time, a different method on the basis of Markov Random Field (MRF) and a hybrid social algorithm consisting of a gossiping algorithm and an Ant Colony Optimization (ACO) is proposed in [72]. Ants find the optimum path between a food source and their nest. This forging behavior of ants is used for heuristic optimization which is a multi-agent guided scheme, called the ACO. In every iteration, the suitable result of each ant is spread rapidly among its neighbors. In the next iteration because of this positive feedback, a purposive path that is closer to the optimal solution can be found. The convergence process speeds up due to this smart behavior. Hence the combination of the gossiping algorithm with ACO aids to find an improved path using neighborhood. Several experiments using this design were performed on phantom and real images.

3.1.8. Miscellaneous methods

A CAD system that detects and classifies the MRI brain tumor images as benign and malignant is presented in [73]. In this, the image sharpening is done on T1-w while anisotropic diffusion filtering is done on the T2-w image. The reason for using an unsharp mask for obtaining a sharp image is that the clarity of the T1-w is explained by its sharpness. Similarly, the anisotropic diffusion filter decreases the loss of information by efficiently preserving detailed structures and object boundaries. The alpha blending technique is used for compositing both axial T1-w and T2-w images. The segmentation of tumor area is done using the Enhanced Watershed Segmentation (EWATS) algorithm. GLCM techniques are used for texture feature extraction from the segmented image. For efficient cataloging Regularized Logistic Regression (RLR) is used.

At the same time in [74], GLCM proved to be the best among the different feature extraction methods based on intensity. The WEKA tool classification algorithm J48 (decision tree algorithm) showed similarity with GLCM features. Similarly [75] explains a tumor extraction method for early and rapid detection of a brain tumor. The tumor area extraction and classification is done with the decision tree classifier which is a non-parametric, rule-based classifier requiring no presumption about variable distribution in each class. Also having the benefits of being simple structured.

Volumetric 3D segmentation, reconstruction, and visualization of brain tumor using axial, sagittal and coronal planes of multimodal brain MRI are explained in [76]. Images were skull stripped and interpolated to an isotropic resolution of 1 mm for every voxel. The intensity difference feature extraction is used. Morphological operations are performed on tumor mask obtained so far in order to refine the content and margin of tumor regions. Initially, the erosion operator is used to remove any residual region around the tumor followed by dilation for filling the holes within the tumor mass.

Glioma classification can be facilitated by perfusion metric as it can't be achieved by conventional MRI alone [51]. This work aims to find the potential of relative Cerebral Blood Flow (rCBF), rCBV and relative Percentage Signal intensity Recovery (rPSR) values of $T2^*$ DSC perfusion MRI, in discriminating HGG and LGG. It was concluded that rPSR inversely correlates while rCBV and rCBF values directly correlate with the tumor grade. DSC perfusion MRI is a widely used for evaluating the hemodynamic characteristics (rCBV and rCBF) of the brain, as it helps in assessing the malignancy of

the tumor. But rPSR is the only parameter among the different perfusion metrics which takes into account the leakage factor for the characterization of heterogeneity of brain tissues. It's clear in [51] that radiologist trust semi-automatic method. The limitation of this work was the manual placement of the ROI for the assessment of different parameters.

A fusion-based technique for segmentation based on a blend of deformable model and spatial relations is proposed in [77]. Three popular deformable methods: snake, level set and distance regularized level set evolution were used for predicting their performance in generating the brain tumor boundaries. Generally, deformable methods require user-initialization. But the initial curve is automatically generated by this proposed method. The work consisted of three stages: initial curve placement is made by Extended Maxima transform, final curve segment is converged using boundary-based deformable models, performance is compared using final curve region with each other.

To characterize the changes in MR signal at the tumor boundary, a boundary analysis method i.e. distinct from basic edge detection was proposed in [78]. The tumor margin status was significantly correlated with boundary distance and slope of T2 signal changes at the normal/tumor tissue boundary. Based on a sampling of the MRI intensity from 90 constructed sampling rays that stem from a point marked by a radiologist, near the midpoint of the tumor, the tumor boundary attributes were measured.

An automatic method using linear vector quantization for brain tumor classification into benign or malignant accompanied with a combination of texture and shape features is proposed in [79]. The feature vector is composed of Fourier Descriptor coefficients (FD) and 7-moment invariants which give shape representation, along with 13 Haralicks texture features. These are input for classification to linear vector quantization which is a supervised variant of Kohonen learning rule.

A data-driven analysis of multi-parametric MR imaging, taking into account the MR imaging heterogeneity of the lesions significantly improves discrimination between low- and high-grade brain gliomas were explained in [80]. It was concluded that this method significantly improved sensitivity and specificity. Basic MRI gives relevant information concerned with the presence of edema, contrast enhancement, multicentricity and/or multifocality, hemorrhage, necrosis, and mass effect, which are all markers of glioma aggressiveness. But because of overlap of MRI features found in LGG and HGG, classification using basic MRI is often uncertain, with sensitivity varying from 55% to 83%.

A computer aided method using Open CV (Open source Computer Vision library) and embedded system for detection of brain tumor tissue was used in [81]. The comparison between open CV and existing methods showed that accuracy was highest and the execution time was the least for this method. Open CV is an open source computer vision and machine learning software library.

3.2. Semi-automatic 2D & 3D user interaction methodologies

3.2.1. FCM

A Unified Model based classification with FCM (UMCF) using Extended Hyperbolic Tangent (EHT) model (derived from logistic regression), Gaussian mixture model and fuzzy soft clustering technique is used in [82]. EHT quantifies the relationship between two variables. Soft clustering minimizes dissimilarities among objects of same cluster and similarity among different classes. Normal cells, edema and tumor were represented by using pixel value 0,100 and 255 respectively. The advantage of this work was that using EHT model reduces false positive and false negative.

For the classification of astrocytomas as WHO, high/low grade, [83] portrays the use of Fuzzy Cognitive Maps (FCMs). It models and represents the knowledge of experts like their expertise, experience, heuristic etc. The powerful properties of neural networks and fuzzy logic are blended into FCMs. It's grading ability and applicability was strengthened by the Activation Hebbian Algorithm (AHL). The most useful experience and knowledge of experts were extracted by AHL algorithm. FCMs benefits were the ample transparency and interpretability in the decision process and drawback was the convergence to undesired regions which was avoided by the use of suitable learning algorithms. Hence when new strategies were adopted, the learning algorithms recalculated the weights. To assess the tumor grade, experts usually utilize 8 histopathological features: cellularity, mitoses, apoptosis, the giant cells, the multinucleated cells, the necrosis, the vascular proliferation and the pleomorphism. These key characteristics encoded the degree of malignancy of the tumor. The experts could qualitatively explain the degree of causality among concepts and need not explain the causality relations by numerical values.

3.2.2. SVM

For the purpose of glioma grading and for distinguishing between metastases and gliomas, a computer-assisted classification scheme fusing the basic MRI and rCBV maps, calculated from perfusion MRI is developed in [84]. SVM-RFE performed the feature subset selection. Two expert neuroradiologists manually traced 4 ROIs, from which the features were extracted. Results show that grading differentiation is possible by incorporating rCBV maps. A drawback was the necessity to trace ROIs making it a semiautomatic approach and causing inter- and intra- observer variability.

A multiclass classification system is used in [42] to determine tumor grade and type. Along with RBF kernel, the Least Squares Support Vector Machines (LS-SVM) were used and correlated with LDA. A data set consisting of 10 classes of pathologies of Magnetic Resonance Spectroscopic Imaging (MRSI) and MRI data are obtained from the INTERPRET project database. MRSI preprocessing steps were a correction for eddy current effects, frequency alignment, filtering of k-space data by a hanning filter and baseline correction using an exponential filter, followed by subtraction of the residual of the original signal. Entire data is preprocessed semi-automatically and images are co-aligned. Registration of image is done with respect to the PD-weighted image by shifting and maximizing the spatial correlation. Further, the results were improved by Automatic Relevance Determination (ARD) for feature selection.

Prediction of the degree of glioma malignancy and selection of appropriate features was done using SVM with floating search method in [85]. For this purpose, the feature subset evaluation was done by the SVM-based wrapper method and for the feature subset generation, the Backward Floating Search (BFS) method was used. BFS is based on SFS which adds the most relevant features one by one and SBS which removes the least relevant feature one by one. This work clearly shows that the feature subsets of distinct data sets provide classification accuracy and not the individual features.

A hybrid system for brain tumor classification using GA and SVM with Gaussian RBF kernel is recommended in [44]. The selection of the most relevant features was done by GA optimization and the experimental output showed that GA improved SVM's classification accuracy from 56.3 to 91.7%. Each feature component was normalized independently to a specified range by linear scaling in the limits of [0,1]. This ensures that the greater value input characteristics do not overwhelm the smaller value inputs hence decreasing prediction error.

For the definition of regions, multidimensional or multispectral segmentation uses information from more than one original image of the same site. [21] proposes a method to inspect the tumor state by measuring its volume change over time, of the same patient. It learns the brain tumor and selects the features, further by using SVM the tumor in new data is segmented automatically. Also, the tumor contour is refined by a region growing technique. Feature

selection is done by optimization of kernel class separability. The adaptive training automatically tracks the tumors due to variations of tumor characteristics over time or acquisition condition.

3.2.3. ANN

A methodology starting with a mouse click on an image identifying and circumscribing the tumor using semi or fully automatic CAD system and finally being acknowledged as a pathological tissue by the physician was proposed in [86]. This system did identification of tumor and quantitative measurements. The AIR (Automatic Image Registration) software was used to align the Diffusion Tensor Imaging (DTI) datasets offline and hence correcting artifacts. On each map, the glioma ROI was drawn manually followed by applying texture analysis on the segmented ROIs. Using a sliding window approach, features were calculated from the gradient histogram and intensity, from GRLM and GLCM. The Fisher-filter score was used to identify the discriminating features per map and per patient. And then PCA was used to cut down redundancy of information. A BPFFNN was used for the supervised classification.

The benign and malignant astrocytic gliomas were differentiated using a three-layer, FFNN with a back propagation algorithm in [87]. MR images were reviewed and graded independently by three neuroradiologists without knowledge about the pathological results. The MR parameter readings of each observer were given into the NN to map them to the equivalent pathological outputs. The performance was better when relative Receiver Operating Characteristic curve (ROC) areas were 0.94 with and 0.91 without radiologists' impression, compared to 0.84 by a radiologist. It took 100 iterations and 562 learning processes to perfectly train the network. The strongest indicator of malignancy among the evaluated features was the presence of ring enhancement having a maximum correlation with pathological findings. The other indicators were tumor heterogeneity, the degree of contrast enhancement and the extent of edema.

To assist radiologists in the multiclass classification of brain tumor, an interactive CAD system was proposed in [33]. Content Based Active Contour (CBAC) model was used to mark the tumor regions which were saved as segmented ROIs. From these segmented ROIs 71, texture and intensity feature set were extracted. A combination of classifiers was used namely ANN using MLP learning algorithm and GA with SVM using Gaussian RBF kernel. The preliminary probability in tumor class identification was provided by GA-SVM, also benefits in accuracy and speed. The joined output from dual classifiers aided the radiologists in improved diagnosis.

In medical images segmentation of homogeneous tumors was done using active contour models based on intensity like Magnetostatic Active Contour (MAC), Gradient Vector Flow (GVF) and Fluid Vector Flow (FVF), but the analysis in [88] shows that many of these schemes decline to segment homogeneous tumors against the identical background. So CBAC was proposed which use both texture and intensity information present inside the active contour. In this method, from 2D slices, tumor volume is extracted and is called as 2.5D segmentation. The contour is guided iteratively towards the boundary of the tumor by Static Motion Field (SMF) and Dynamic Motion Field (DMF).The dynamic field aims to deform the contour to cover the tumor while the static field makes the contour reach the boundary of the tumor. To guide the contour toward the tumor boundary SMF uses gradient force if the contour lies outside the tumor boundary. Finally using static and dynamic fields, CBAC makes the active contour to segment the tumor.

A user interactive model for primary and secondary brain tumor extraction which is a boundary based technique called GVF is used in [39]. PCA-ANN approach classifies these segmented ROIs. Gradient Descent Back-Propagation with Momentum (GDBPM) algorithm is used for judging weights in the training phase. These tumors are manually segmented and graded by an expert for validation.

A multiclass brain tumor classification using PCA-ANN approach is done with a diversified dataset in [30]. Being a semiautomatic scheme, the radiologist marked the ROIs initially. 856 ROIs were segmented using CBAC model. The initial contour is used by CBAC to find texture and intensity values outside and inside ROI. Three sets of experiments were performed. Firstly, classification accuracy was checked using ANN approaches. Secondly, the segmented ROIs of the same patient were repeated during testing and PCA-ANN approach with random sub-sampling was used. The classification accuracy increased from 77 to 91%. Thirdly the segmented ROIs of the same patients were not common for testing and training sets. This was done to check the proposed systems robustness and for bias removal hence resulting in 85.23% overall accuracy.

Brain tumor discrimination is done fusing a non-linear Least Squares Features Transformation (LSFT) with PNN classifier in [48]. By conditioning the textural features using LSFT, the performance of PNN classifier was boosted significantly at the same time resulting in dimensionality reduction and increased class separability. At the initial level of the decision tree, metastatic and primary brain tumors are distinguished and in next level meningioma and glioma, resulting in a two-level hierarchical decision tree. Two distinct LSFT-PNN classifiers were used for classification at each level of the decision tree. A cubic and a quadratic LSFT-PNN was employed at the first level and at the second level of the decision tree respectively. The non-parametric Wilcoxon rank sum test was used for feature dimensionality reduction. Two cross-validations were done, the Leave-One-Out method (LOO) and the External Cross-Validation (ECV) method.

3.2.4. Miscellaneous methods

In [89] how to differentiate the factors that separate or define a grade of the tumor by use of MRI is showcased. 36 pathologically verified gliomas were analyzed and compared with biopsy diagnosis to find out if MRI could be used to classify astrocytic tumors to low-grade astrocytoma, anaplastic astrocytoma, and glioblastoma multiforme. The MR features evaluated were border definition, mass effect, edema, tumor signal heterogeneity, hemorrhage, necrosis or cyst formation and crossing of the middle line.

Based on minimum user interaction, a semi-automatic method using kNN segments by training and generalizing within brain only is proposed in [23]. A merit to be noted in this method is that without human interruption any new brain can be processed, once training is done. On the other side, a drawback is that data might have been collected from distinct MRI scanners for training on multiple brain subjects. This gave rise to a problem with the MR image intensities as it is not consistent over various MRI scanners. This work reveals that CRF is a substitute to MRF and kNN-CRF gave improved performance than kNN and kNN-MRF. The processing using kNN-CRF and kNN-MRF techniques took within one and two minutes per brain.

K-means algorithm is used for segmentation initially in [90] but it fails to handle noise on the data and outliers. Hence watershed segmentation was used to separate the tumor cells from the healthy cells. The watershed method has a drawback that it is highly sensitive to local minima.

In [26] initially, the radiologist visually identifies the salient region which was used to segment the brain lesion accurately. Automatically applying salient information as labeling constraints quickened the N-Cut segmentation. Segmentation by saliency weighted N-Cut segmentation demonstrates a brain MRI analysis technique that would determine the scientific value of images with no training requirement. The McStrip method was used to remove non-brain parts. Features like multi-scale contrast, motion perception and curvature feature were used. The Graph-based Visual

Saliency (GVBS) and Saliency for Image Manipulation (SIM) were the software used (for comparison Matlab implementation was also used).

The consolidated details of the reviewed works are tabularized in Tables 1 and 2. Table 1 consolidates the method of user interaction, preprocessing, feature extraction, the number of features, feature types, dimensionality reduction methods, segmentation methodologies, classifiers opted and their outputs, classes/tumor types and performance evaluation. Table 2 summarizes the modalities, dataset and sources of the database used. The works having no techniques used under a heading have been marked as NA-Not Applied/NM- Not Mentioned.

4. Discussion

Most of the reviewed works focused on automatic methods. Vastly used preprocessing methods involved median filtering, N4ITK for bias correction, skull stripping using BET, Image sharpening, registration and anisotropic diffusion filtering, scoring the maximum usage. Most of the algorithms especially the conventional FCM algorithm is sensitive to noise in the MR image, so the focus must be on reducing the negative effect from Rician noise, which is the common type of noise in MR images [3].

This survey reveals that segmentation was done mainly using CNN, FCM, SOM, CBAC and MRF. Brain MRI segmentation methods can be classified into 6 major categories- Threshold Based Segmentation (eg: Otsu method and Th-mean method), Region Based Segmentation (eg: Region splitting, merging and growing), Edge Detection, Clustering (hard and soft clustering, algorithms used FCM and K-means), Statistical Models(EM algorithm, MRF model) and ANN [11]. It is stated in [91] also that the most commonly used techniques for tumor analysis were based on FCM, region growing, fuzzy sets and hybrid. Due to the rise in varying specifications and new applications, selecting the most appropriate technique confined to a particular application is difficult. In such cases, a combination of different techniques can be done to fulfill the desired segmentation goal. Hence, in current scenario hybrid or combination of segmentation methods are used so as to avoid the disadvantages of each method alone, which will improve the segmentation accuracy.

Hybrid techniques that combine two or more techniques and soft computing techniques like NN, fuzzy logic and GA have found wide applications in image segmentation. Reference [11] gives a review on the various hybrid segmentation methods revealing that K-means has better performance and less computational complexity. Hence by applying K-means in conjunction with other methods, it is possible to increase the segmentation performance.

Summarizing the feature extraction techniques surveyed, the most commonly used method was DWT and GLCM. PCA and GA scored the highest usage for dimensionality reduction. The misclassifications can be diminished by concentrating on high dimensional features including pathological and radiological tumor details [33].

The classification was mostly performed using PNN, RF, SVM, CNN, MRF, ANN, SOM and fuzzy methodologies, while classification with hybrid systems gave the best accuracy. Classifiers such as SVM and, lately RF were favorably used for brain tumor segmentation [66]. The natural capability of RF in handling large feature vectors and multi-class problems made it popular. The MICCAI-BRATS Challenge reveals that methods relying on RF are among the most accurate [4]. Research shows a good performance on CNN-based algorithms especially in the field of 2D data classification. The merit of CNN is that each kernel in different layers is learned spontaneously, so that there is no need of feature setting beforehand because of which, the number of training example becomes critical [67].

Table 1
Summary of algorithms followed for classification/segmentation and their performance analysis

Paper	User interaction	preprocessing	Feature extraction	Segmentation + Classification	classes/tumor type	Performance evaluation
[2]	A	median, unsharp masking and wiener filter	Thresholding method	T2PCM + Type-II Approximate Reasoning method	WM, GM, CSF, Abnormality	accuracy- 83
[13]	2D-A	median filter and high pass filter	DWT + PCA	FPCNN + ANN	Normal, abnormal	accuracy- 99, OF- 92, specificity- 100
[16]	2D & 3D-A	N4ITK	CNN	DNN	non-tumor, necrosis, edema, non-enhancing tumor and enhancing tumor	dice (tumor regions: complete- 0.88, core- 0.79 and enhancing- 0.73), OF (tumor regions: complete- 0.87, core- 0.79 and enhancing- 0.80), specificity (tumor regions: complete- 0.89, core- 0.79 and enhancing- 0.68), speed- 25 s to 3mins
[31]	2D-A	Skull stripping	mean, magnitude and direction	K Means & FCM clustering method + RBF, GRNN, PNN, FPNNC	tumorous, nontumorous	accuracy- 98, OF- 97.9, specificity- 96.9, speed- (kmean-0.273, FCM-2.9887)
[33]	2D-A	does not require pre-processing	86 features + CFS	Rough entropy based thresholding in granular computing paradigm + RF	Glioblastoma multiforme, metastasis, meningioma and granuloma	accuracy- 95, OF- (GBM-96.7, MET-96.2, MG-98.1 and GN-97.7)

[34]	2D-SA	NA	71 intensity and texture feature set + GA	CBAC + SVM & ANN	dataset 1-Astrocytoma, Glioblastoma Multiforme, Medulloblastoma, Meningioma and Metastatic, dataset 2-Astrocytoma, Low Grade Glioma and Meningioma	accuracy- (first dataset: GA-SVM-91.7 and GA-ANN 94.9, second dataset: GA-SVM 89 and GA-ANN 94.1), training time- 1 h & 2 h, testing time- 0.70 & 0.60 ms
[35]	2D-SA	NA	NA	EHT + UMCF	normal, edema, tumor	HG-(accuracy- 100, precison-0.95, recal- 0.98); LG-(accuracy- 100, precision- 0.98, recal- 0.92)
[36]	2D-A	Images under each moment are very robust to noise.	moment invariant + binary AR	NN & AR-NN	normal, benign, malignant	accuracy- (NN-73.3, AR-NN-83.72), precision- (NN- for normal: 0.9245; for benign: 0; for malignant: 0.7938. AR-NN- for normal: 0.8302; for benign: 0.5455; for malignant: 0.9027), OF- (NN- for normal: 0.6049; for benign: NaN; for malignant: 0.8462. AR-NN- for normal: 0.7586; for benign: 0.7059; for malignant: 0.9027), specificity- (NN- for normal: 0.9560; for benign: 0.8721; for malignant: 0.7531. AR-NN- for normal: 0.9211; for benign: 0.9355; for malignant: 0.8800)
[37]	2D & 3D-A	skull stripping using BET and ROI based brain masking	Interpolation of mean and variance	SOM based FKM clustering	malignant and benign, tumor and edema	accuracy- 96.18, MSE- 2.151, PSNR-41.85 dB, dice- 47.36, SI- 0.9189, JI-31.54, EF- 0.0256, OF- 0.8718, specificity- 0.9737, speed- 2.8s
[38]	2D-A	NA	DSD-MSA	PSO, DPSO, or FODPSO + SVM	healthy and unhealthy brain MRIs	accuracy- 99.18, UQI- 0.4536, OF-100, specificity- 97.95, speed- 4.57s
[39]	2D-A	Image sharpening & anisotropic diffusion filtering	GLCM	EWATS + RLR	benign and malignant	accuracy- 96, NAE- 0.08468, PSNR-24.85, SS- 0.978, NCC— 0.94924, OF- 97, specificity- 86
[40]	3D-A	bias field removal, equalization, skull stripping and interpolation to isotropic resolution.	Intensity Difference Feature Extraction	3D volumetric, intensity based segmentation	NA	Dice- 0.76, OF- 84.645, specificity-98.232
[41]	2D-A	NA	Statistical features and Gabor wavelet features + PCA (475 to 20 features)	sliding window + SVM, KNN, SRC, NSC, k-means clustering	tumor and healthy tissue	accuracy- 97.4, OF- 96.2, specificity- 95.7, speed- (Tumor slice detection: 12 min, Gabor wavelet feature extraction: 17 min, Statistical feature extraction: 18 min, PCA on Gabor wavelet feature: 59 min, PCA on statistical feature: 11 min)
[42]	2D-A	anisotropic diffusion filter	intensity, LBP, GLCM, and wavelet characteristics, Law's energy texture features and also Features extracted from biopsy	canny edge detection method + ANFIS	healthy and abnormal (benign or malignant)	SI-0.817, OF-0.82, EF- 0.182, PPV-0.817
[43]	2D-A	registeration, Otsu thresholding	NA	FCM, KFCM	tumour, non-tumour	OF- 64.84, specificity- 99.89, Dice-71.83
[44]	2D-A	de-noising by median filter and Skull removal by BSE	NA	thresholding and level set + KIFCM	NA	accuracy- (dataset 1- 90.5, dataset 2- 100, dataest 3- 100), precision-(100 for all datasets), recall-(dataset 1- 90.5, dataset 2- 100, dataest 3- 100), speed- (dataset 1-12.87s, dataset 2- 5.18s, dataset 3-3.46s)

Table 1 (*Continued*)

Paper	User interaction	preprocessing	Feature extraction	Segmentation + Classification	classes/tumor type	Performance evaluation
[45]	SA	AIR software	sliding-window approach + PCA	FFBPNN	tumor voxels were classified into 3 classes	AUC- (p map- 0.96, FA map- 0.98), OF- (p map- 90, FA map- 92.6), specificity- (p map- 90, FA map- 92.6), classification error- (p map- 10.0, FA map- 7.3)
[46]	2D-SA	BET, FLIRT from FSL	t-test with bagging, constrained LDA, SVM-RFE (161 to 50 features)	LDA with Fisher's discriminant rule, k-NN, nonlinear SVMs	meningioma, glioma of grades II, III, IV and metastasis	accuracy- 91.2, AUC- 93.6
[47]	2D-A	Image resizing, RGB to grayscale conversion	Wavelet Features, GLCM Features, Law's Energy Texture Features	ANFIS	benign and malignant	Accuracy-99.4, SI- 0.78, PPV- 99.06, NPV- 99.41, Specificity- 99.98, OF- 72.39, EF- 0.0098, speed- 0.441 s
[49]	2D & 3D-A	median filtering, unsharp masking, histogram equalization, FLIRT	feature ranking using information gain, feature selection using ICA, PCA, GA, 2D & 3D feature extraction using Haar wavelet (432-dimensional feature vector)	DWT, MFCM + SVM, ANN, kNN	benign and malignant	accuracy- 99.09, VO- 89.35, HD- 3.62, SMD- 0.54 mm, OF- 100, specificity- 98.21, speed- (with reduced feature set- 4–5 s, with complete feature vector- 12 s)
[50]	2D-A	T2FIE	CFC	Interval Type-2 fuzzy set theory and relative entropy + Interval Type-2 approximate reasoning method	Astrocytomas grade I-IV	Accuracy- 89, precision- 99, OF- 89, specificity- 90
[52]	2D & 3D-A	NA	The 6 volumetric features from multidimensional co occurrence matrix and 3 spectroscopic features from metabolite ratios	ELM-IPSO neural network classifier	pathological tissues (tumor and edema), normal tissues (WM and GM), fluid-CSF, HGG and LGG	accuracy- 99.15, MSE- 0.015, AUC- 0.97, OF- 98.01, specificity- 95
[55]	3D-SA	co-registration, filtering of k-space data by a Hanning filter, correction for eddy current effects, frequency alignment and a simple baseline correction using an exponential filter, subtraction of the residual of the original signal.	feature selection- Fisher discriminant criterion, Kruskal-Wallis test, Relief-F and ARD for Bayesian LS-SVM (10 features/spectrum)	LS-SVM-RBF, LDA	1- normal tissue, 2- CSF, 3- grade II diffuse astrocytomas, 4- grade II oligoastrocytomas, 5- grade II oligodendrogliomas, 6- grade III astrocytomas, 7- grade III oligoastrocytomas, 8- grade III oligodendrogliomas, 9- meningiomas, 10- grade IV gliomas.	accuracy- 98.24, Brier score- 2.9179 exp −3
[56]	2D-A	RGB to gray conversion, resizing	PCA	PNN	dataset 1- Normal, Benign and Malignant, dataset 2- Glioma and Meningioma	accuarcy- (dataset 1- for SV = 10e6 is 65.71 and for SV = 10e7 is 97.14, dataset 2- for SV = 10e5 is 90 and for SV = 10e6 is 100), OF- (dataset 1- for SV = 10e6 is 76.92 and for SV = 10e7 is 92.30, dataset 2- for SV = 10e5 is 85.7 and for SV = 10e6 is 100), specificity- (dataset 1- for SV = 10e6 is 59 and for SV = 10e7 is 100, dataset 2- for SV = 10e5 is 100 and for SV = 10e6 is 100)
[57]	2D-SA	NA	manually 13 features	FFBPNN	malignant and benign astrocytic gliomas	AUC- 0.9408, accuracy- 92, SSE- 0.02, speed- (562 learning processes, 100 iterations in each learning process within 2 h)

[58]	SA	NA	manually by histopahologists	fuzzy cognitive maps	LG & HG astrocytomas	accuracy- (LG- 90.26, HG- 93.22), OF- 93.22, specificity- 92.68
[59]	2D-A	denoising by Nl means filter, Brain extraction using EM algorithm followed by dilatation.	NA	decision tree classifier	tumor and non tumor	accuracy- 0.912, DSC- 0.913, JSC- 0.9, precision- 0.936, OF- 0.899, specificity- 0.975, speed- 1 min
[60]	2D-A	artefact removal and noise reduction	histogram based features,and texture based features using GLCM (13 features)	ANFIS	5 types- Glioma, Meningioma, Metastatic adenocarcinoma, Metastatic bronchogenic carcinoma, and Sarcoma	accuracy- 98.25, error rate- 0.05, Kappa Index- 0.9, Jacard index- 0.89
[62]	2D-SA	NA	LoG, GLCM, RILBP, DGTF, IBF, RICGF (218 intensity and texture features) + PCA	CBAC + PCA-ANN	6 classes- astrocytoma, glioblastomamultiforme, childhood tumor-medulloblastoma, meningioma, secondary tumor-metastatic, normal regions	accuracy- 91, speed- training time- 25 min, testing time- 0.55 ms
[63]	3D-A	dwFCM reduces the negative effects of rician noise	LaV deformation features, intensity features	dwFCM + ANN, SVM	background, WM, GM, CSF, tumor, edema	Accuracy- (SVM: 98.9, ANN:98.8), Miss rate- (SVM:10.0, ANN:11.7)
[65]	2D-A	For noise removing and anti-blurring a Gaussian Filter is used	histogram, GLCM, J48 and intensity	J48 (decision tree algorithm) classifier	Tumor (Metastatic bronchogenic carcinoma, Astrocytoma, Meningioma, sarcoma) and normal class	accuracy- (for intensity histogram- 89, GLCM-95.25, J48- 97.5, intensity- 93), MCC- (for intensity histogram- 0.84, GLCM- 0.96, J48- 0.98, intensity- 0.92)
[66]	2D-A	BEA	NA	ExM transform (Extended Maxima), Parametric Deformable model (snakes), Geometric deformable model (Level set Function), DRLSM	CSF, WM, GM and background	Jaccard, William's index- calculated individually
[67]	2D-A	bias field correction by N4ITK method, intensity normalization	To train the CNNs for HGG and LGG, 450,000 and 335,000 patches, respectively were extracted	CNN	normal tissue, necrosis, edema, non-enhancing, enhancing tumor	Dice- (BRATS 2013 dataset- for the complete, core, and enhancing regions are 0.88, 0.83, 0.77,BRATS 2015 dataset- 0.78, 0.65, 0.75), speed- 8 min
[70]	2D-SA	NA	36 textural features- 4 features from the ROI's histogram, 22 from the Co-occurrence Matrices and 10 from the run-length matrices + non-parametric Wilcoxon rank sum test (36 to 10 features)	LSFT-PNN classifier (first level- cubic, second level- quadratic)	metastatic and primary brain tumors (gliomas and meningiomas)	accuracy- (first level cubic LSFT-PNN classifier- 94.03, second level quadratic LSFT-PNN classifier- 99.33), OF- 93.48, specificity- 95.24, speed- 40 min
[72]	2D & 3D-A	NA	Optimal Symmetric Multivariate Templates, Asymmetry and Symmetric Template Normalization features, Voxelwise Image Features for RF Segmentation, Intensity Modeling and Regional Geometry features	RF + MRF	CSF, GM, WM, edema, non-enhancing tumor, enhancing tumor, and abnormal necrotic center or necrocyst in HGG	Dice- (challenge dataset: complete- 0.87, core- 0.78, enhanced- 0.74), positive predictive value- (challenge dataset: complete- 0.85, core- 0.74, enhanced- 0.69), OF- (challenge dataset: complete- 0.89, core- 0.88, enhanced- 0.83), speed- 2hours
[73]	2D-SA	normalize the data to the quadrant of [−1, 1]	Wrapper on SVMs + BFS gave 15 features reduced to 6 features	SVMs, ANNs, FMMNN-FRE	LG, HG	Accuracy- (87.14 for dataset1 and 88.33 for dataset2 by SVMs vs. 83.21 for dataset1 and 86.37 for dataset2 by FMMNN-FRE)
[75]	2D-A	enhancement filter	13 Haralick texture feature	FFBPNN, RNN, Elman network	Oligodendroglioma, Meningioma and Glioblastoma	BP NN and RNN- performance ratio was 76.47, for Elman 88.24

Table 1 (*Continued*)

Paper	User interaction	preprocessing	Feature extraction	Segmentation + Classification	classes/tumor type	Performance evaluation
[76]	3D-SA	registeration and alignment	Manually 6 simple features	kNN, kNN-MRF, kNN-CRF	edema, non-enhancing tumor, enhancing tumor and healthy tissue	Dice- (kNN-CRF: complete- 0.85 core- 0.75 enhancing- 0.63), precision- (kNN-CRF: complete- 0.92 core-0.84 enhancing- 0.77), recall- (kNN-CRF: complete- 0.80 core- 0.73 enhancing-0.56), speed- 1 min
[79]	2D-A	Median Filter, Pulse-coupled neural network	GLCM, PCA and statistical methods (Shape based feature- 4 Intensity based features- 5 Texture based features- 6) + SFLA	FCM & Watershed segmentation + SVM, LVQ, Naive Bayes	LG, HG astrocytoma	accuracy- (SVM- 88.88, LVQ- 91.67, Naive Bayes- 91), error- (SVM- 11.12, LVQ- 8.33, Naive Bayes- 9), speed- (SVM- 0.5286s, LVQ- 0.1572s, Naive Bayes- 0.0342s)
[81]	2D-A	Median filter	10 features- 8 GLCM features & 2 features are patients' identity based.	FBB + FFBPNN	Grade II-IV	accuracy- (Grade I- 93.93, Grade II- 97.77, Grade III- 94.22)
[82]	2D-A	ROIs obtained using FCM clustering technique, rCBV maps were created from the DSC MR data using standard kinetic models, normalization	rCBV histogram parameters with patient age gives 101 features + PCC, PCA, ICA	FCM + SVM	LGG & HGG	accuracy- (PCA- 85, PCC- 82, ICA- 79), OF- (PCA- 89, PCC- 89, ICA- 87), specificity- (PCA- 84, PCC- 77, ICA- 75), speed- (PCA- 0.076s, PCC- 0.067s, ICA- 0.094s)
[83]	2D-SA	NA	GLCM, LoG, DGTF, RICGF, RILBP, Intensity based features- 218 texture and intensity features + PCA	GVF + ANN (Gradient Descent Back-Propagation algorithm)	6 classes- primary tumor-Astrocytoma, Glioblastoma Multiforme, child tumor-Medulloblastoma, Meningioma, secondary tumor-Metastatic along with normal regions	accuracy- 95.37
[84]	2D-SA	NA	GLCM, LoG, DGTF, RICGF, RILBP, Intensity based features, Shape based Feature- 71 features + GA	SVM-GRBF	five classes- Primary tumors- Astrocytoma, Glioblastoma Multiforme, Meningioma, child tumor –Medulloblastoma along with secondary tumor- Metastatic	accuracy- 91.7
[85]	2D-A	NA	DWT- 4761 coefficients	SOM, SVM	normal or abnormal brain	accuracy- (SOM- 94, SVM-linear- 96.15, SVM-polynomial- 98, SVM-RBF- 98)
[86]	2D-A	NA	DWT + PCA (1024 features to 7 features)	FFBPNN, kNN	normal or abnormal	accuracy- (ANN – 97, kNN-98.6), MSE- 0.00001, OF- (ANN- 98.3, kNN- 100), specificity- (ANN- 90, kNN- 90)
[88]	3D-A	noise removal by binary mask, BET	overlapping windows, GLCM, Moment invariants + GA (24 features reduced to 5)	k-means + HFS-SOM, EGS-SOM	WM, GM, CSF	MSE- 0.03
[89]	2D-A	Histogram Equalization, Binarization, Morphological Operations	GLCM + GA + fuzzy rough set (20 features reduced to 7)	ANFIS	Astrocytoma grade I to IV	OF- 96.9, specificity- 95.6, accuracy- 97
[90]	2D-A	Anisotropic diffusion filter	SWT, spatial filtering	SOM, LVQ	GM, WM and other	TC- (WM- 0.5481, GM- 0.6548), Dice- (WM- 0.7001, GM- 0.7880)
[91]	2D-A	NA	Slantlet transform, intensity histogram- 6 features	BPNN	normal brain or a pathological brain, suffering from Alzheimer's disease.	accuracy- 100, speed- feature extraction- 0.39 s, neural network training- 1.26s, implementation phase- 5.946 ms (per image)
[92]	2D-SA	McStrip	Multi-scale contrast, Curvature feature, Motion perception	saliency weighted N-Cut segmentation	normal and tumorous	accuracy- 83.4 – 95, AUC—- 0.76, SM- 0.59, CC- 0.53
[93]	3D-A	binary mask, sliding window	overlapped sliding window, Haralick features, Hu moments- (24 first, second order and invariant features) + PCA, NSGA-2	GHSOM with probability-based clustering	WM, GM, CSF or Background	TI calculated individually

[94]	3D-SA	median filter to remove intensity irregularities	GLCM	CBAC using SMF and DMF estimation	five different types of homogeneous, heterogeneous, diffused tumors	speed- 2 to 5s
[96]	3D-A	Anisotropic diffusion filter for RF inhomogeneity correction,	the square of intensity, the Euclidean distance between pixels	Skull stripping by VFC + 3 SVM classifiers	WM, GM and CSF	average of absolute error value of GM- 1.6, WM- 3.9, speed- 1 h
[97]	2D & 3D-A	Anisotropic diffusion filtering, local entropy minimization and a bicubic spline model method (LEMS)	NA	MsFCM, k-means	three tissue types (labeled as Classes I, II, and III)	Synthetic images- overlap ratios of 85 for CSF, 84 for GM, 92 for WM, Real MR images- overlap ratios of 85 for CSF, 82 for GM, 88 for WM, speed- 3mins
[99]	3D-A	NA	NA	MRF-ACO- Gossiping algorithm	NA	DSC- IBSR dataset-0.664 Brainweb dataset-0.762, speed- IBSR dataset–144 s Brainweb dataset–238 s
[100]	2D-A	NA	DWT + PCA (1024 features reduced to 19)	BPNN + SCG	normal or abnormal	accuracy- 100, speed- 0.0452s
[101]	2D & 3D-SA	registeration using SPM	windowing- 26 features, 2DWT, feature-selection by optimization of kernel class separability	Multi-kernel SVM	normal or abnormal	error- 0.109, accuracy- 95
[102]	2D-A	NA	Haar wavelet + PCA (1024 features reduced to 19)	FFNN optimized via ACPSO	normal or abnormal	accuracy- 98.75, MSE- 1E-29, speed- 0.0452 s
[103]	2D-A	NA	Fourier descriptor coefficients (FD), moment invariants, Haralicks texture features- (Texture attributes:13, shape attributes:98)	Linear Vector Quantization	malignant or benign	accuracy- 85, speed- 16.64 s
[105]	2D-A	intensity normalization	self-learned features obtained from CNN	CNN	LG, HG	OF and specificity with intersected value of 0.6667
[107]	2D-A	NA	GLCM + GLRM + fuzzy entropy measure	FFNN, MLP, BPNN	normal or abnormal	Accuracy- (FFNN- 76.19, MLP- 85.09, BPNN- 96.7), OF- (FFNN- 82.3, MLP- 76, BPNN- 72), Specificity- (FFNN- 88.23, MLP- 86.75, BPNN- 84)

Abbreviations: A- Automatic; SA- Semi-Automatic; 2D-A- 2 Dimensional Automatic; 2D-SA- 2 Dimensional Semi Automatic; 3D-A- 3 Dimensional Automatic; 3D-SA- 3 Dimensional Semi Automatic; 2D & 3D-A- 2 Dimensional & 3 Dimensional Automatic; 2D & 3D-SA- 2 Dimensional & 3 Dimensional Semi Automatic; WM- White Matter; GM- Grey Matter; CSF- cerebrospinal fluid;RGB- Red Green Blue; DSC- Dynamic Susceptibility Contrast; Dice/DOI- Dice Similarity Coefficient/Dice Overlap Index; MSE- Mean Square Error; PSNR- Peak Signal to Noise Ratio; JI/TC- Jaccard (TanimotoCoeffecient) Index; SI- Similarity Index;OF- Overlap Fraction/Sensitivity/Recall; EF- Extra Fraction; UQI- Universal Quality Index; NAE- Normalized Absolute Error; SS- Structural Similarity; NCC- Normalized Cross-Correlation;PPV- Positive Predictive Value; NPV- Negative Predictive Value; AUC- Area Under the Receiver Operating Characteristic Curve; VO- Volume Overlap;HD- Hausdorff Distance; SMD- Symmetric Mean Absolute Surface Distance; SSE- Sum Square Error; JSC- Jaccard's Similarity Coefficient; SV- Spread Value; BEA- Brain Extraction Algorithm; MCC- Mathews Correlation Coefficient; SM- Similarity Measure; CC- Correlation Coefficient; T2PCM- Type II Possibilistic C-Mean; DWT- Discrete Wavelet Transform; PCA- Principal Component Analysis; FPCNN- Feedback Pulse Coupled Neural Network; FFNN- Feed Forward Neural Network; ANN- Artificial Neural Network; CNN- Convolutional Neural Networks; DNN- Deep Convolutional Neural Networks; GRNN- Generalized Regression Neural Network; RBF- Radial Basis Function; PNN- Probabilistic Neural Network; FPNNC- Fuzzy Probabilistic Neural Network Classifier; CFS- Correlation based Feature Set; RF- Random Forest; CBAC- Content Based Active Contour; GA- Genetic Algorithm; EHT- Extended Hyperbolic Tangent; UMCF- Unified Model based Classification with FCM; HG- High Grade; LG- Low Grade; AR- Association Rule; NN- Neural Network; AR-NN- Association Rule Based Neural Network; SOM- Self Organizing Maps; PSO- Particle Swarm Optimization; DPSO- Darwinian Particle Swarm Optimization; FODPSO- Fractional Order DPSO; DSD-MSA- Directional Spectral Distribution-Multi Scale Analysis; EWATS- Enhanced Watershed Segmentation; RLR- Regularized Logistic Regression; GLCM- Gray Level Co-occurrence Matrix; SVM- Support Vector Machine; kNN- k Nearest Neighbour; SRC- Sparse Representation Classifier; NSC- Nearest Subspace Classifier; LBP- Local Binary Patterns; ANFIS- Adaptive Neuro-Fuzzy Inference System; FCM- Fuzzy C-Means; KFCM- Kernelized Fuzzy C-Means; BSE- Brain Surface Extractor; KIFCM- K-Means Integrated with Fuzzy C-Means; FFANN- Feed Forward Artificial Neural Network; FMMNN-FRE- Fuzzy Rule Extraction based on Fuzzy Min–Max Neural Networks; BET- Brain Extraction Tool; ROI- Region of Interest; FKM-Fuzzy K-Means; SVM-RFE- Support Vector Machine-Recursive Feature Elimination;DWT- Discrete Wavelet Transforms; MFCM- Modified FCM ;CFC- Collaborative Fuzzy Clustering; T2FIE- Type 2 Fuzzy Image Enhancement; ELM-IPSO- Extreme Learning Machine-Improved Particle Swarm Optimization; LS-SVM-RBF Least Squares Support Vector Machines With Radial Basis Function; ARD-Automatic Relevance Determination; LDA- Linear Discriminant Analysis; SMF- Static Motion Field; DMF- Dynamic Motion Field; VFC- Vector Field Convolution; PNN- Probabilistic Neural Network; Nl means- Non-local means; EM- Expectation Maximization; LoG- Laplacian of Gaussian; RILBP- Rotation Invariant Local Binary Patterns; DGTF- Directional Gabor Texture Features; IBF- Intensity Based Features; RICGF- Rotation Invariant Circular Gabor Features; LaV- Lateral Ventricle; dwFCM- dynamically wavelet incorporated FCM; DRLSM- Distance Regularized Level Set Method; LSFT-PNN- Least Squares Features Transformation-Probabilistic Neural Network; RF- Random Forest; MRF- Markov Random Field; CRF- Conditional Random Field; BFS- Backward Floating Search;RNN- Recurrent Neural Networks; SFLA- Shuffling Frog Leaping Algorithm; FBB- Fast Bounding Box;FFBPNN- Feed Forward Back Propagation Network; PCC- Pearson's Correlation Coefficients; PCA- Principal Component Analysis; ICA- Independent Component Analysis; GVF- Gradient Vector Flow; GRBF- Gaussian Radial Basis Function; HFS-SOM- Histogram Fast Volume Segmentation SOM; EGS-SOM- Entropy Gradient Segmentation SOM; SWT- Stationary Wavelet Transforms;LVQ- Learning Vector Quantization;BPNN- Back Propagation Neural Networks; Mcstrip- Minneapolis Consensus Strip; NSGA-2- Non-dominated Sorting Genetic Algorithm; GHSOM- Growing Hierarchical Self-Organizing Map; VCF- Vector Field Convolution; MsFCM- Multiscale Fuzzy C-Means; MRF-ACO- Markov Random Field- Ant Colony Optimization; ACPSO- Adaptive Chaotic Particle Swarm Optimization; SPM- Statistical Parametric Mapping; GLRM- Gray Level Run Length Matrix; MLP- Multilayer Perceptron; HGG- High-Grade Glioma; LGG- Low-Grade Glioma; rCBV- relative Cerebral Blood Volume; GBM- Glioblastoma Multiforme; MET- Metastasis; MG- Meningioma; GN- Granuloma; AIR- Automatic Image Registration; P map- isotropic component map of the diffusion tensor; FA map- Fractional Anisotropy map of the diffusion tensor; FSL- FMRIB Software Library; FLIRT- FSL Linear Image Registration Tool; SCG- Scaled Conjugate Gradient; IBSR- Internet Brain Segmentation Repository; NA- Not Applicable; NM- Not Mentioned.

Table 2
Review of data collection.

Paper	Modalities	Dataset used(N/A)	Database
[2]	T1w	95 patients	NA
[13]	axial, T2w	256-256 pixel	Harvard
[16]	T1, T2, T1C, FLAIR	30 patient (20 HG, 10 LG)	BRATS 2013
[31]	NA	50 images	NA
[33]	T1C	360	EKO CT & MRI Scan Centre at Medical College and Hospitals Campus, Kolkata
[34]	T1C	428 of 55 patients, 260 of 10 patients	dataset 1- PGIMER; dataset 2- Harvard
[35]	T1w, T2w, T1c, FLAIR	5 different slices of 22 high grade and 15 low-grade tumors (=185) and 20 synthetic data	BRAT 2012
[36]	T1c	172	IBSR
[37]	Coronal, sagittal and axial T1w, T2w, FLAIR	38 images	KGS Advanced MR & CT Scan – Madurai, Tamilnadu, India & Harvard Brain Repository.
[38]	axial T2w	30 normal, 20 abnormal	Harvard
[39]	axial T1w, T2w	106 T1, 53 T2-w	Government General Hospital, Puducherry, India, Christian Medical College, Vellore, India and Devi Scans, Thiruvananthapuram, India.
[40]	T1w, T2w, T1c	10	BRATS2012
[41]	T1w, FLAIR	25 real and simulated MR images (181 slices/subject)	NCI-MICCAI 2013
[42]	NA	200	NA
[43]	T1w, T1c, FLAIR	20	NA
[44]	T1, T2, PDw, FLAIR, T1c	255	DICOM, Brain Web data set, BRATS
[45]	T2w FSE (Fast Spin Echo), T1w FFE(fast field echo)	15 patients (9 LG, 6 HG) and 6 healthy patients	San Raffaele Hospital, Milan
[46]	Axial 3D T1w, sagittal 3D T2w, FLAIR, Axial 3D T1wce, T2*w dynamic susceptibility perfusion MRI	98 patients, 102 brain tumors	NA
[47]	NA	NA	open access web Source www.brainweb.org.
[49]	T1c, T2w	550 patients, 64 slices/patient, 550 patients, 280 benign tumors, 270 malignant tumors	ShirdiSai Cancer Hospital, Manipal, India
[50]	axial T1w	95 MRI scans- 85 patients with Astrocytomas, 10 normal patients	NA
[52]	T1w, T1c, 1H-MRSI	35 patients; 12 meningiomas and 23 gliomas	PSG IMSR & Hospitals, Coimbatore, Tamilnadu, India
[55]	T1w, T2w, PDw, T1c, MRSI	25 patients with brain tumor, 4 normal patients	INTERPRET project database and the University Medical Center Nijmegen (UMCN)
[56]	NA	Dataset 1- 70 training samples, 35 testing samples, Dataset 2- 24 training samples, 20 testing samples	Government Hospital of Aurangabad and Sahyadri Hospital of Pune, Maharashtra, India
[57]	Tlw, Tlwc, T2w	129 training sets(43*3 reader), 43 patients, 33 malignant, 10 benign Test set- 36 patients(1 reader)	NA
[58]	NA	100 cases- 41LG, 59 HG	Department of Pathology of the University Hospital of Patras, Greece
[59]	T1w	65 images	40 Brain web data, 25 IBSR V2.0
[60]	T2w, T2c	320 slices	Harvard
[62]	T1w	428 MR images from 55 patients, 428 normal regions (NR).	Department of Radiodiagnosis, Postgraduate Institute of Medical Education and Research (PGIMER), Chandigarh, India
[63]	T1w, T2w, T1Cw, Flair	660,000 data points from 11 cases	Whole Brain Atlas of med.harvard and MICCAI 2012 Challenge on Multimodal Brain Tumor Segmentation-BRATS2012
[65]	NA	250 brain tumor MRI images	BRATS
[66]	axial T2w	10 slices	whole brain atlas (WBA) maintained by Harvard medical school
[67]	T1, T1c, T2, FLAIR	BRATS 2013- 65 MR scans BRATS 2015- 327 MR scans	BRATS 2013 and 2015
[70]	T1w	67 MR images	General Hellenic Airforce Hospital, MRI Unit, Katehaki, Athens, Greece
[72]	FLAIR, T1w, T1c, T2w	30 glioma patients, 10 LG, 20 HG	BRATS 2013
[73]	T1, T2	DS1-280 glioma (169 LG, 111 HG), DS2- 154 cases (85 LG, 69 HG)	Hua–Shan Hospital in Shanghai of China.
[75]	T1, T2	NA	State University of Campinas, School of Medicine (FCMUNICAMP), Campinas, Brazil
[76]	T1c, T2, FLAIR	30 patient (20 HG, 10 LG), 30 simulated subjects	BRATS 2013
[79]	T2w	200 images- 164 trainig set (82 LG, 82HG), 36 testing set (18 LG, 18HG)	Dr.Shajis MRI & Medical Research 709 Centre Pvt.Ltd, Puthiyara, Calicut
[81]	NM	130 MR images- 33 Grade II, 44 Grade III, 53 Grade IV	NM
[82]	T2w, T1w, T1c, (DSC)	101 patients, 63 HG, 38 LG	NA
[83]	T1c	55 patients, 428 MR images, 856 ROIs	Department of Radiodiagnosis, Postgraduate Institute of Medical Education & Research (PGIMER), Chandigarh, India
[84]	T1c	55 patients, 428 MR images	Department of Radiodiagnosis, Postgraduate Institute of Medical Education & Research (PGIMER), Chandigarh, India

Table 2 (*Continued*)

Paper	Modalities	Dataset used(N/A)	Database
[85]	axial T2w	52 MR brain images- 6 normal brains, 46 abnormal brains (affected by Alzheimer's disease)	Harvard
[86]	axial T2w	70, 60 abnormal, 10 normal	Harvard
[88]	T1w volumetric images	IBSR 1.0- 20 images, IBSR 2.0- 18 images	IBSR 1.0, IBSR 2.0
[89]	NM	NM	web resource http://mouldy.bic.mni.mcgill.ca/brainweb/
[90]	T1-w	20 normal people	IBSR database
[91]	axial T2w	75 transaxial image slices (39 normal brains, 36 pathological brain, suffering from Alzheimer's disease)	Harvard
[92]	Dataset 1- T1w, T2w, PDw	dataset 3- 25 patients with gliomas	dataset 1- Brain web tumor repository, dataset 2- Harvard medical school, dataset 3- radiology department of Pakistan Institute of Medical Sciences (PIMS)
	Dataset 2- T1w		
	Dataset 3- T1w, T2w		
[93]	axial, coronal, sagittal T1w	20 images	IBSR
[94]	T1w, T1c, T2w	dataset1- 428 images of 45 subjects, dataset2-, 260 images of 10 subjects	dataset1- PGIMER, dataset2- Harvard
[96]	T1w	10 MR images	Internet-connected MRI simulator at the McConnell Brain Imaging Centre in Montreal
[97]	T1w, T2w, PDw	30 synthetic images	synthetic images and McGill brain MR database (McConnel Brain Imaging Center, McGill University, Quebec, Canada)
[99]	T1w, T2w, PDw (single and multispectral MRIs)	Dataset 1- 20 normal MRI	Dataset 1- Internet Brain Segmentation Repository (IBSR), by the Center for Morphometric Analysis (CMA) at Massachusetts General Hospital
		Dataset 2- simulated 3D MR images	Dataset 2- BrainWeb Simulated Brain Dataset from the McGill University
[100]	axial T2w	66 images- 18 normal, 48 abnormal	Harvard
[101]	T2w, PDw, FLAIR	11 patients	CHU de Caen and Tiantan Hospital, Beijing
[102]	axial T2w	160 images (20 normal, 140 abnormal)	Harvard
[103]	NA	80 images- 40 malignant, 40 benign	open source database and some hospitals
[105]	NA	195 patient- 170 HG, 25 LG	BRATS 2014
[107]	NA	42 patients- 25 abnormal, 17 normal	NA

An approach to be highlighted is the Deep Learning which deals with learning complex features automatically and directly from data. A review in [34] about the high performances of deep learning methods reveals that it can be considered as the current state-of-the-art for glioma segmentation. Reference [44] concluded that in forthcoming research works, a dataset consisting of class like Glioma and subclasses like high and low-grade Astrocytoma must be gathered for classification. Also, it is seen that [92], 7T MRI contributes to the additional insight of pathogenesis of brain tumor paving path for new treatment developments.

Lastly, because glioma grade depends on the appearance of MR images, tumor segmentation model must exclude contrasts enhanced blood vessels and include tumor areas with contrast enhancement [20]. Also to keep track of tumor growth or recurrence, repeated invasive procedures are uncommon, making non-invasive methods common. But at the same time, automatic methods has to be closely equivalent to radiologist perception [22]. If this is unachievable by a fully automatic method, interactive i.e. semi-automatic methods that can be user initialized come into the picture.

5. Conclusion

A consolidated review on the recent segmentation and classification techniques on Brain MR Images gathers the knowledge that early detection of a brain tumor and its grade is a stepping stone to further studies. The digital image processing methodologies along with machine learning techniques aid radiologists in efficient diagnosis, as hybrid techniques provide a second opinion and assistance to them. The review has focused on the latest trends in segmentation and classification of tumor-bearing human brain MR images having gliomas which include astrocytoma. The methodologies used in various approaches were discussed with an intention for applying practically these methods for clinical application. This survey brings to the notice that though there is the achievement of high classification accuracy, these techniques were tested on two broad categories of malignant and benign/Low Grade and High Grade and further classification of tumor types like WHO grading system was not considered. This review is designed leaving trails towards the development of an image processing and machine learning approach dedicated towards grading of brain tumor especially the most incident of gliomas: Astrocytomas.

Declaration of interest

There is no conflict of interest with other people or organizations within three years of beginning the submitted work that could inappropriately influence, or be perceived to influence, their work.

Funding

This research did not receive any specific grant from funding agencies in the public, commercial, or not-for-profit sectors.

Acknowledgements

We are grateful to School of Electronics Engineering, School of Electrical Engineering and the management, VIT University for the immense support in piloting this review.

References

[1] M. Horn, Magnetic Resonance Imaging Methods and Biologic Applications, Humana Press, New Jersey, 2006, http://dx.doi.org/10.1385/1597450103.
[2] N.J. Tustison, K.L. Shrinidhi, M. Wintermark, C.R. Durst, B.M. Kandel, J.C. Gee, M.C. Grossman, B.B. Avants, Optimal symmetric multimodal templates and concatenated random forests for supervised brain tumor segmentation (simplified) with ANTsR, Neuroinformatics 13 (2015) 209–225, http://dx.doi.org/10.1007/s12021-014-9245-2.

[3] S.L. Jui, S. Zhang, W. Xiong, F. Yu, M. Fu, D. Wang, A.E. Hassanien, K. Xiao, Brain MRI tumor segmentation with 3D intracranial structure deformation features, IEEE Intell. Syst. 31 (2016) 66–76, http://dx.doi.org/10.1109/MIS.2015.93.
[4] B.H. Menze, A. Jakab, S. Bauer, J. Kalpathy-Cramer, K. Farahani, J. Kirby, Y. Burren, N. Porz, J. Slotboom, R. Wiest, L. Lanczi, E. Gerstner, M.A. Weber, T. Arbel, B.B. Avants, N. Ayache, P. Buendia, D.L. Collins, N. Cordier, J.J. Corso, A. Criminisi, T. Das, H. Delingette, C. Demiralp, C.R. Durst, M. Dojat, S. Doyle, J. Festa, F. Forbes, E. Geremia, B. Glocker, P. Golland, X. Guo, A. Hamamci, K.M. Iftekharuddin, R. Jena, N.M. John, E. Konukoglu, D. Lashkari, J.A. Mariz, R. Meier, S. Pereira, D. Precup, S.J. Price, T.R. Raviv, S.M.S. Reza, M. Ryan, D. Sarikaya, L. Schwartz, H.C. Shin, J. Shotton, C.A. Silva, N. Sousa, N.K. Subbanna, G. Szekely, T.J. Taylor, O.M. Thomas, N.J. Tustison, G. Unal, F. Vasseur, M. Wintermark, D.H. Ye, L. Zhao, B. Zhao, D. Zikic, M. Prastawa, M. Reyes, K. Van Leemput, The multimodal brain tumor image segmentation benchmark (BRATS), IEEE Trans. Med. Imaging 34 (2015) 1993–2024, http://dx.doi.org/10.1109/tmi.2014.2377694.
[5] R.C. Gonzalez, R.E. Woods, Digital Image Processing, second ed., Prentice Hall, New Jersey, 2002.
[6] I.N. Bankman, Handbook of Medical Imaging, Processing and Analysis, Academic Press, CA, 2000.
[7] A. Ortiz, J.M. Gorriz, J. Ramirez, D. Salas-Gonzalez, J.M. Llamas-Elvira, Two fully-unsupervised methods for MR brain image segmentation using SOM-based strategies, Appl. Soft Comput. J. 13 (2013) 2668–2682, http://dx.doi.org/10.1016/j.asoc.2012.11.020.
[8] Z. Ji, Q. Sun, Y. Xia, Q. Chen, D. Xia, D. Feng, Generalized rough fuzzy c-means algorithm for brain MR image segmentation, Comput. Methods Programs Biomed. 108 (2012) 644–655, http://dx.doi.org/10.1016/j.cmpb.2011.10.010.
[9] H. Wang, B. Fei, A modified fuzzy C-means classification method using a multiscale diffusion filtering scheme, Med. Image Anal. 13 (2009) 193–202, http://dx.doi.org/10.1016/j.media.2008.06.014.
[10] K.S. Thara, K. Jasmine, Brain tumour detection in MRI images using PNN and GRNN, IEEE WiSPNET 2016 Conf., IEEE (2016) 1504–1510.
[11] P.S. Shijin Kumar, V.S. Dharun, A study of MRI segmentation methods in automatic brain tumor detection, Int. J. Eng. Technol. 8 (2016) 609–614.
[12] S. Prima, N. Ayache, T. Barrick, N. Roberts, Maximum likelihood estimation of the bias field in MR brain images: investigating different modelings of the imaging process, in: Med. Image Comput. Comput. Interv. – MICCAI 2001 4th Int. Conf., Springer, Berlin, Heidelberg, Utrecht, The Netherlands, 2001, pp. 811–819, http://dx.doi.org/10.1007/3-540-45468-3_97.
[13] M.G. Ballanger, E. Biglieri, S. Furui, Y.-F. Huang, N. Jayant, A.K. Katsaggelos, M. Kaveh, P.K.R. Rajasekaran, J.A. Sorenson, Signal Processing and Communications, Taylor & Francis, Boca Raton, 2005.
[14] E. Abdel-Maksoud, M. Elmogy, R. Al-Awadi, Brain tumor segmentation based on a hybrid clustering technique, Egypt. Informatics J. 16 (2015) 71–81, http://dx.doi.org/10.1016/j.eij.2015.01.003.
[15] N. Nabizadeh, M. Kubat, Brain tumors detection and segmentation in MR images: gabor wavelet vs statistical features, Comput. Electr. Eng. 45 (2015) 286–301, http://dx.doi.org/10.1016/j.compeleceng.2015.02.007.
[16] E.-S.A. El-Dahshan, H.M. Mohsen, K. Revett, A.-B.M. Salem, Computer-aided diagnosis of human brain tumor through MRI: a survey and a new algorithm, Expert Syst. Appl. 41 (2014) 5526–5545, http://dx.doi.org/10.1016/j.eswa.2014.01.021.
[17] S. Koley, A.K. Sadhu, P. Mitra, B. Chakraborty, C. Chakraborty, Delineation and diagnosis of brain tumors from post contrast T1-weighted MR images using rough granular computing and random forest, Appl. Soft Comput. J. 41 (2016) 453–465, http://dx.doi.org/10.1016/j.asoc.2016.01.022.
[18] S. Chaplot, L.M. Patnaik, N.R. Jagannathan, Classification of magnetic resonance brain images using wavelets as input to support vector machine and neural network, Biomed. Signal Process. Control. 1 (2006) 86–92, http://dx.doi.org/10.1016/j.bspc.2006.05.002.
[19] G. Liberman, Y. Louzoun, O. Aizenstein, D.T. Blumenthal, F. Bokstein, M. Palmon, B.W. Corn, D. Ben Bashat, Automatic multi-modal MR tissue classification for the assessment of response to bevacizumab in patients with glioblastoma, Eur. J. Radiol. 82 (2013) e87–e94, http://dx.doi.org/10.1016/j.ejrad.2012.09.001.
[20] K.E. Emblem, B. Nedregaard, J.K. Hald, T. Nome, P. Due-Tonnessen, A. Bjornerud, Automatic glioma characterization from dynamic susceptibility contrast imaging: brain tumor segmentation using knowledge-based fuzzy clustering, J. Magn. Reson. Imaging 30 (2009) 1–10, http://dx.doi.org/10.1002/jmri.21815.
[21] N. Zhang, S. Ruan, S. Lebonvallet, Q. Liao, Y. Zhu, Kernel feature selection to fuse multi-spectral MRI images for brain tumor segmentation, Comput. Vis. Image Underst. 115 (2011) 256–269, http://dx.doi.org/10.1016/j.cviu.2010.09.007.
[22] S. Bauer, R. Wiest, L.-P. Nolte, M. Reyes, A survey of MRI-based medical image analysis for brain tumor studies, Phys. Med. Biol. 58 (2013) R97–R129, http://dx.doi.org/10.1088/0031-9155/58/13/R97.
[23] M. Havaei, P.M. Jodoin, H. Larochelle, Efficient interactive brain tumor segmentation as within-brain kNN classification, Proc. – Int. Conf. Pattern Recognit., Published by Institute of Electrical and Electronics Engineers Inc. (2014) 556–561, http://dx.doi.org/10.1109/ICPR.2014.106.
[24] K. Somasundaram, T. Kalaiselvi, Fully automatic brain extraction algorithm for axial T2-weighted magnetic resonance images, Comput. Biol. Med. 40 (2010) 811–822, http://dx.doi.org/10.1016/j.compbiomed.2010.08.004.
[25] Y. Zhu, G.S. Young, Z. Xue, R.Y. Huang, H. You, K. Setayesh, H. Hatabu, F. Cao, S.T. Wong, Semi-automatic segmentation software for quantitative clinical brain glioblastoma evaluation, Acad. Radiol. 19 (2012) 977–985, http://dx.doi.org/10.1016/j.acra.2012.03.026.
[26] I. Mehmood, N. Ejaz, M. Sajjad, S.W. Baik, Prioritization of brain MRI volumes using medical image perception model and tumor region segmentation, Comput. Biol. Med. 43 (2013) 1471–1483, http://dx.doi.org/10.1016/j.compbiomed.2013.07.001.
[27] B. Tanoori, Z. Azimifar, A. Shakibafar, S. Katebi, Brain volumetry: an active contour model-based segmentation followed by SVM-based classification, Comput. Biol. Med. 41 (2011) 619–632, http://dx.doi.org/10.1016/j.compbiomed.2011.05.013.
[28] M.H. Fazel Zarandi, M. Zarinbal, M. Izadi, Systematic image processing for diagnosing brain tumors: a type-II fuzzy expert system approach, Appl. Soft Comput. J. 11 (2011) 285–294, http://dx.doi.org/10.1016/j.asoc.2009.11.019.
[29] V.R. Simi, J. Joseph, Segmentation of glioblastoma multiforme from MR images – a comprehensive review, Egypt. J. Radiol. Nucl. Med. 46 (2015) 1105–1110, http://dx.doi.org/10.1016/j.ejrnm.2015.08.001.
[30] J. Sachdeva, V. Kumar, I. Gupta, N. Khandelwal, C.K. Ahuja, Segmentation, feature extraction, and multiclass brain tumor classification, J. Digit. Imaging 26 (2013) 1141–1150, http://dx.doi.org/10.1007/s10278-013-9600-0.
[31] K.R. Swanson, C. Bridge, J.D. Murray, E.C. Alvord, Virtual and real brain tumors: using mathematical modeling to quantify glioma growth and invasion, J. Neurol. Sci. 216 (2003) 1–10, http://dx.doi.org/10.1016/j.jns.2003.06.001.
[32] J. Egger, T. Kapur, A. Fedorov, S. Pieper, J.V. Miller, H. Veeraraghavan, B. Freisleben, A.J. Golby, C. Nimsky, R. Kikinis, GBM volumetry using the 3D Slicer medical image computing platform, Sci. Rep. 3 (2013) 1364, http://dx.doi.org/10.1038/srep01364.
[33] J. Sachdeva, V. Kumar, I. Gupta, N. Khandelwal, C.K. Ahuja, A package-SFERCB-Segmentation, feature extraction, reduction and classification analysis by both SVM and ANN for brain tumors, Appl. Soft Comput. J. 47 (2016) 151–167, http://dx.doi.org/10.1016/j.asoc.2016.05.020.
[34] A. Isın, C. Direkoglu, M. Sah, Review of MRI-based brain tumor image segmentation using deep learning methods, in: 12th Int. Conf. Appl. Fuzzy Syst. Soft Comput. ICAFS, Procedia Computer Science, Vienna, Austria, 2016, pp. 317–324, http://dx.doi.org/10.1016/j.procs.2016.09.407.
[35] G. Vishnuvarthanan, M.P. Rajasekaran, P. Subbaraj, A. Vishnuvarthanan, An unsupervised learning method with a clustering approach for tumor identification and tissue segmentation in magnetic resonance brain images, Appl. Soft Comput. J. 38 (2016) 190–212, http://dx.doi.org/10.1016/j.asoc.2015.09.016.
[36] B. Menze, M. Reyes, A. Jakab, E. Gerstner, J. Kirby, J. Kalpathy-Cramer, K. Farahani, NCI-MICCAI challenge on multimodal brain tumor segmentation, in: Proc NCI-MICCAI BRATS, Nagoya, Japan, 2013.
[37] D.S. Chow, J. Qi, X. Guo, V.Z. Miloushev, F.M. Iwamoto, J.N. Bruce, A.B. Lassman, L.H. Schwartz, A. Lignelli, B. Zhao, C.G. Filippi, Semiautomated volumetric measurement on postcontrast MR imaging for analysis of recurrent and residual disease in glioblastoma multiforme, Am. J. Neuroradiol. 35 (2014) 498–503, http://dx.doi.org/10.3174/ajnr.A3724.
[38] S. Andrews, G. Hamarneh, A. Saad, Fast random walker with priors using precomputation for interactive medical image segmentation, in: T. Jiang, N. Navab, J.P.W. Pluim, M.A. Viergever (Eds.), Med. Image Comput. Comput. Interv. – MICCAI 2010 13th Int. Conf. Proc., Springer Science & Business Media, Beijing, China, 2010, pp. 9–16, http://dx.doi.org/10.1007/978-3-642-15711-0_2.
[39] V. Kumar, J. Sachdeva, I. Gupta, N. Khandelwal, C.K. Ahuja, Classification of brain tumors using PCA-ANN, in: Proc. 2011 World Congr. Inf. Commun. Technol. WICT 2011, IEEE, Mumbai, India, 2011, pp. 1079–1083, http://dx.doi.org/10.1109/WICT.2011.6141398.
[40] D. Zikic, B. Glocker, E. Konukoglu, A. Criminisi, C. Demiralp, J. Shotton, O.M. Thomas, T. Das, R. Jena, S.J. Price, Decision forests for tissue-specific segmentation of high-grade gliomas in multi-channel MR, Med. Image Comput. Comput. Interv. 15 (2012) 369–376, http://dx.doi.org/10.1007/978-3-642-33454-2_46.
[41] M. Havaei, A. Davy, D. Warde-Farley, A. Biard, A. Courville, Y. Bengio, C. Pal, P.M. Jodoin, H. Larochelle, Brain tumor segmentation with deep neural networks, Med. Image Anal. 35 (2017) 18–31, http://dx.doi.org/10.1016/j.media.2016.05.004.
[42] J. Luts, A. Heerschap, J.A.K. Suykens, S. Van Huffel, A combined MRI and MRSI based multiclass system for brain tumour recognition using LS-SVMs with class probabilities and feature selection, Artif. Intell. Med. 40 (2007) 87–102, http://dx.doi.org/10.1016/j.artmed.2007.02.002.
[43] F.G. Zollner, K.E. Emblem, L.R. Schad, SVM-based Glioma grading: optimization by feature reduction analysis, J. Med. Phys. 22 (2012) 205–214, http://dx.doi.org/10.1016/j.zemedi.2012.03.007.
[44] J. Sachdeva, V. Kumar, I. Gupta, N. Khandelwal, C.K. Ahuja, Multiclass brain tumor classification using GA-SVM, Dev. E—Syst. Eng. 97 (2011) 182–187, http://dx.doi.org/10.1109/DeSE.2011.31.
[45] M. Sharma, S. Mukharjee, Brain tumor segmentation using hybrid genetic algorithm and artificial neural network fuzzy inference system (ANFIS), Int. J. Fuzzy Log. Syst. 2 (2012) 31–42.
[46] P. Ganeshkumar, P. Shanthakumar, Performance analysis of classifier for brain tumor detection and diagnosis, Comput. Electr. Eng. 45 (2015) 302–311, http://dx.doi.org/10.1016/j.compeleceng.2015.05.011.
[47] M.M. Subashini, S.K. Sahoo, V. Sunil, S. Easwaran, A non-invasive methodology for the grade identification of astrocytoma using image processing and artificial intelligence techniques, Expert Syst. Appl. 43 (2016) 186–196, http://dx.doi.org/10.1016/j.eswa.2015.08.036.

[48] P. Georgiadis, D. Cavouras, I. Kalatzis, A. Daskalakis, G.C. Kagadis, K. Sifaki, M. Malamas, G. Nikiforidis, E. Solomou, Improving brain tumor characterization on MRI by probabilistic neural networks and non-linear transformation of textural features, Comput. Methods Programs Biomed. 89 (2008) 24–32, http://dx.doi.org/10.1016/j.cmpb.2007.10.007.
[49] A. Ortiz, J.M. Gorriz, J. Ramirez, D. Salas-Gonzalez, Improving MRI segmentation with probabilistic GHSOM and multiobjective optimization, Neurocomputing 114 (2013) 118–131, http://dx.doi.org/10.1016/j.neucom.2012.08.047.
[50] S. Roy, S. Sadhu, S.K. Bandyopadhyay, D. Bhattacharyya, T.H. Kim, Brain tumor classification using adaptive neuro-fuzzy inference system from MRI, Int. J. Biol.—Sci. Biol.—Technol. 8 (2016) 203–218, http://dx.doi.org/10.14257/ijbsbt.2016.8.3.21.
[51] K.A. Smitha, A.K. Gupta, R.S. Jayasree, Relative percentage signal intensity recovery of perfusion metrics-an efficient tool for differentiating grades of glioma, Br. J. Radiol. 88 (2015), http://dx.doi.org/10.1259/bjr.20140784.
[52] I. Jolliffe, Principal component analysis, in: Wiley StatsRef Stat Ref. Online, 2014, pp. 1–5, http://dx.doi.org/10.1002/9781118445112.stat06472.
[53] C. Fernandez-Lozano, J.A. Seoane, M. Gestal, T.R. Gaunt, J. Dorado, C. Campbell, Texture classification using feature selection and kernel-based techniques, Soft Comput. 19 (2015) 2469–2480, http://dx.doi.org/10.1007/s00500-014-1573-5.
[54] M.P. Arakeri, G.R. Mohana Reddy, Computer-aided diagnosis system for tissue characterization of brain tumor on magnetic resonance images, Signal Image Video Process. 9 (2013) 409–425, http://dx.doi.org/10.1007/s11760-013-0456-z.
[55] M. Zarinbal, M.H. Fazel Zarandi, I.B. Turksen, M. Izadi, A type-2 fuzzy image processing expert system for diagnosing brain tumors, J. Med. Syst. 39 (2015) 110, http://dx.doi.org/10.1007/s10916-015-0311-6.
[56] P. Szwarc, J. Kawa, M. Rudzki, E. Pietka, Automatic brain tumour detection and neovasculature assessment with multiseries MRI analysis, Comput. Med. Imaging Graph. 46 (2015) 178–190, http://dx.doi.org/10.1016/j.compmedimag.2015.06.002.
[57] A. Lakshmi, T. Arivoli, Computer aided diagnosis system for brain, J. Theor. Appl. Inf. Technol. 64 (2014) 561–567.
[58] A. Thiyagarajan, U. Pandurangan, Comparative analysis of classifier performance on MR brain images, Int. Arab J. Inf. Technol. 12 (2015) 772–779, http://dx.doi.org/10.3923/ijscomp.2013.199.206.
[59] E.S.A. El-Dahshan, T. Hosny, A.B.M. Salem, Hybrid intelligent techniques for MRI brain images classification, Digit. Signal Process. 20 (2010) 433–441, http://dx.doi.org/10.1016/j.dsp.2009.07.002.
[60] B. Sudha, P. Gopikannan, A. Shenbagarajan, C. Balasubramanian, Classification of brain tumor using neural network, Proc. World Congr. Eng. 2014 WCE 2014 (2014) 673–678.
[61] E. Hussein, D. Mahmoud, Brain tumor detection using artificial neural networks, J. Sci. Technol. 13 (2012) 31–39, http://www.sustech.edu/staff_publications/20130323072020220.pdf.
[62] Y. Sharma, C. Megha, An improved automatic brain tumor detection system: int, J. Adv. Res. Comput. Sci. Softw. Eng. 5 (2015) 11–15.
[63] M. Maitra, A. Chatterjee, A Slantlet transform based intelligent system for magnetic resonance brain image classification, Biomed. Signal Process. Control. 1 (2006) 299–306, http://dx.doi.org/10.1016/j.bspc.2006.12.001.
[64] Y. Zhang, Z. Dong, L. Wu, S. Wang, A hybrid method for MRI brain image classification, Expert Syst. Appl. 38 (2011) 10049–10053, http://dx.doi.org/10.1016/j.eswa.2011.02.012.
[65] S.B. Gaikwad, M.S. Joshi, Brain tumor classification using principal component analysis and probabilistic neural network, Int. J. Comput. Appl. 120 (2015) 5–9.
[66] S. Pereira, A. Pinto, V. Alves, C.A. Silva, Brain tumor segmentation using convolutional neural networks in MRI images, IEEE Trans. Med. Imaging 35 (2016) 1240–1251, http://dx.doi.org/10.1109/tmi.2016.2538465.
[67] Y. Pan, W. Huang, Z. Lin, W. Zhu, J. Zhou, J. Wong, Z. Ding, Brain tumor grading based on neural networks and convolutional neural networks, Eng. Med. Biol. Soc. (EMBC), 2015 37th Annu. Int. Conf. IEEE (2015) 699–702, http://dx.doi.org/10.1109/EMBC.2015.7318458.
[68] A. Demirhan, I. Guler, Combining stationary wavelet transform and self-organizing maps for brain MR image segmentation, Eng. Appl. Artif. Intell. 24 (2011) 358–367, http://dx.doi.org/10.1016/j.engappai.2010.09.008.
[69] S. Lahmiri, Glioma detection based on multi-fractal features of segmented brain MRI by particle swarm optimization techniques, Biomed. Signal Process. Control. 31 (2017) 148–155, http://dx.doi.org/10.1016/j.bspc.2016.07.008.
[70] D.S. Nachimuthu, A. Baladhandapani, Multidimensional texture characterization: on analysis for brain tumor tissues using MRS and MRI, J. Digit. Imaging 27 (2014) 496–506, http://dx.doi.org/10.1007/s10278-013-9669-5.
[71] Y. Zhang, S. Wang, L. Wu, A novel method for magnetic resonance brain image classification based on adaptive chaotic PSO, Prog. Electromagn. Res. 109 (2010) 325–343, http://dx.doi.org/10.2528/PIER10090105.
[72] S. Yousefi, R. Azmi, M. Zahedi, Brain tissue segmentation in MR images based on a hybrid of MRF and social algorithms, Med. Image Anal. 16 (2012) 840–848, http://dx.doi.org/10.1016/j.media.2012.01.001.
[73] D. Aju, R. Rajkumar, T1-T2 weighted MR image composition and cataloguing of brain tumor using regularized logistic regression, J. Teknol. 9 (2016) 149–159.
[74] B.S. Kumar, R.A. Selvi, Feature extraction using image mining techniques to identify brain tumors, IEEE Spons. 2nd Int. Conf. Innov. Inf. Embed. Commun. Syst. ICIIECS'15, IEEE (2015).
[75] S. Sandabad, Y.S. Tahri, A. Benba, A. Hammouch, Novel automatic tumor extraction method based on decision Tree Classifier, Int. J. Eng. Technol. 8 (2016) 75–82.
[76] M. Gupta, B.V.V.S.N.P. Rao, V. Rajagopalan, A. Das, C. Kesavadas, Volumetric segmentation of brain tumor based on intensity features of multimodality magnetic resonance imaging, IEEE Int. Conf. Comput. Commun. Control. IC4 2015 (2015), http://dx.doi.org/10.1109/IC4.2015.7375550.
[77] T. Kalaiselvi, K. Somasundaram, S. Vijayalakshmi, A novel self initiating brain tumor boundary detection for MRI, Commun. Comput. Inf. Sci. 283 (2012) 54–61, http://dx.doi.org/10.1007/978-3-642-28926-2.
[78] T.L. Richards, J.F. Eary, F. O'Sullivan, E.U. Conrad, A method for characterizing sarcoma tumor boundary scanned with T2-weighted MRI, J. Biomed. Graph. Comput. 1 (2011) 1–9, http://dx.doi.org/10.5430/jbgc.v1n1p1.
[79] N. Marshkole, B.K. Singh, A.S. Thoke, Texture and shape based classification of brain tumors using linear vector quantization, Int. J. Comput. Appl. 30 (2011) 21–23.
[80] M. Caulo, V. Panara, D. Tortora, P.A. Mattei, C. Briganti, E. Pravatà, S. Salice, A.R. Cotroneo, A. Tartaro, Data-driven grading of brain gliomas: a multiparametric MR imaging study, Radiology 272 (2014) 494–503, http://dx.doi.org/10.1148/radiol.14132040.
[81] E.T.M.S. Raj, M. Kumaresan, Boundary detection algorithm for brain tumor position and area detection using OPENCV, Int. J. Appl. Eng. Res. 11 (2016) 5326–5331.
[82] U. Maya, K. Meenakshy, Unified Model based classification with FCM for brain tumor segmentation, 2015 IEEE Int. Conf. Power, Instrumentation, Control Comput (2015) 7–10.
[83] E.I. Papageorgiou, P.P. Spyridonos, D.T. Glotsos, C.D. Stylios, P. Ravazoula, G.N. Nikiforidis, P.P. Groumpos, Brain tumor characterization using the soft computing technique of fuzzy cognitive maps, Appl. Soft Comput. 8 (2008) 820–828, http://dx.doi.org/10.1016/j.asoc.2007.06.006.
[84] E.I. Zacharaki, S. Wang, S. Chawla, D.S. Yoo, R. Wolf, E.R. Melhem, C. Davatzikos, Classification of brain tumor type and grade using MRI texture and shape in a machine learning scheme, Magn. Reson. Med. 62 (2009) 1609–1618, http://dx.doi.org/10.1002/mrm.22147.
[85] G.Z. Li, J. Yang, C.Z. Ye, D.Y. Geng, Degree prediction of malignancy in brain glioma using support vector machines, Comput. Biol. Med. 36 (2006) 313–325, http://dx.doi.org/10.1016/j.compbiomed.2004.11.003.
[86] G. De Nunzio, M. Donativi, G. Pastore, L. Bello, R. Soffietti, A. Falini, A. Castellano, Automatic segmentation and therapy follow-up of cerebral glioma in diffusion-tensor images, CIMSA 2010 – IEEE Int. Conf. Comput. Intell. Meas. Syst. Appl. Proc. (2010) 43–47, http://dx.doi.org/10.1109/CIMSA.2010.5611767.
[87] P. Abdolmaleki, F. Mihara, K. Masuda, L.D. Buadu, Neural networks analysis of astrocytic gliomas from MRI appearances, Cancer Lett. 118 (1997) 69–78, http://dx.doi.org/10.1016/S0304-3835(97)00233-4.
[88] J. Sachdeva, V. Kumar, I. Gupta, N. Khandelwal, C.K. Ahuja, A novel content-based active contour model for brain tumor segmentation, Magn. Reson. Imaging 30 (2012) 694–715, http://dx.doi.org/10.1016/j.mri.2012.01.006.
[89] B.L. Dean, B.P. Drayer, C.R. Bird, R.A. Flom, J.A. Hodak, S.W. Coons, R.G. Carey, Gliomas: classification with MR imaging, Radiology 174 (1990) 411–415, http://dx.doi.org/10.1148/radiology.174.2.2153310.
[90] A. Nandi, Detection of human brain tumour using MRI image segmentation and morphological operators, 2015 IEEE Int. Conf. Comput. Graph. Vis. Inf. Secur. (2015) 55–60, http://dx.doi.org/10.1109/CGVIS.2015.7449892.
[91] M.S. Norhashimah, S.A.R. Syed Abu Bakar, A. Sobri Muda, M. Mohd Mokji, Review of brain lesion detection and classification using neuroimaging analysis techniques, J. Teknol. 6 (2015) 73–85.
[92] A.G. Van Der Kolk, J. Hendrikse, J.J.M. Zwanenburg, F. Visser, P.R. Luijten, Clinical applications of 7 T MRI in the brain, Eur. J. Radiol. 82 (2013) 708–718, http://dx.doi.org/10.1016/j.ejrad.2011.07.007.